

國立交通大學

電信工程研究所

碩士論文

以非對稱直交分合波器
設計跨接耦合器及其雙頻設計

New Crossover Coupler Design Using Asymmetric
Branch-Line Hybrids and Its Dual-Band Operation

研究生：詹麒宏 (Chi-Hung Chan)

指導教授：郭仁財 博士 (Dr. Jen-Tsai Kuo)

中華民國 九十九年 七月

以非對稱直交分合波器
設計跨接耦合器及其雙頻設計

New Crossover Coupler Design Using Asymmetric
Branch-Line Hybrids and Its Dual-Band Operation

研究生：詹麒宏
指導教授：郭仁財 博士

Student : Chi-Hung Chan
Advisor : Dr. Jen-Tsai Kuo

國立交通大學
電信工程研究所
碩士論文



Submitted to Department of Communication Engineering

Institute of Electrical and Computer Engineering

National Chiao Tung University

In partial Fulfillment of the Requirements

for the Degree of

Master of Science

In

Communication Engineering

July 2010

Hsinchu, Taiwan, Republic of China

中華民國 九十九 年 七 月

以非對稱直交分合波器 設計跨接耦合器及其雙頻設計

研究生： 詹麒宏

指導教授： 郭仁財 教授

國立交通大學 電信工程研究所

摘要

本論文研究串接兩個任意功率輸出比例的非對稱分波直交耦合器，設計跨接耦合器。每一個耦合器兩個對角端埠可具有不一樣的負載阻抗。由於電路有數個設計自由度，本文以區塊 $ABCD$ 矩陣分析，以預測跨接耦合器的頻寬。

為了讓跨接耦合器具有雙頻功能，本文引用一個基本雙埠單元，取代直交分波耦合器中的四分之一波長傳輸線。此雙埠基本單元包含一段步階式阻抗線段及其末端的兩個並聯傳輸線殘段。利用傳輸線理論，列出解析方程式並求電路參數解。本文實作一個 0.9/1.8 GHz 的跨接耦合器電路，並加以量測以驗證本文所提之設計。

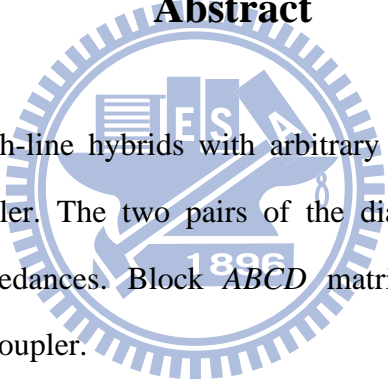
New Crossover Coupler Design Using Asymmetric Branch-Line Hybrids and Its Dual-Band Operation

Student : Chih-Hung Chan

Advisor : Dr. Jen-Tsai Kuo

Institute of Communication Engineering
National Chiao Tung University

Abstract



Two asymmetric branch-line hybrids with arbitrary power divisions are cascaded for design of a crossover coupler. The two pairs of the diagonal ports are allowed to have different characteristic impedances. Block *ABCD* matrices are applied to estimate the bandwidth of the crossover coupler.

To achieve the dual-band operation, an elementary two-port is employed to replace the $\lambda/4$ -section of each hybrid. The two-port consists of a stepped-impedance section with two open stubs shunt at both of its ends. By means of the transmission-line theory, analytical equations are formulated to solve the circuit parameters. A circuit designed at 0.9/1.8 GHz is realized and measured to validate the idea.

Acknowledgement

致謝

研究所這兩年，從無到學富微波知識，最感謝的是我的指導教授，郭人財老師，謝謝老師耐心指導駑鈍如我這般的學生，總是比我還仔細想著研究的每個細節，想法總是那麼富有創意，跟著老師一步一步學，到如今我也能有自己的研究方式和態度，這是我學到最寶貴的資產。同時感謝百忙抽空前來的口試委員：張盛富老師、鐘世忠老師和金國生老師，對學生研究進一步的討論和指導，讓我有更進步的空間。

同時，實驗室同學們，若沒你們的支持和幫助，我根本不可能這麼順利完成論文。逸群學長和裕豪學長，你們學富五車的知識讓我能盡情從你們身上挖掘，當研究遇到瓶頸時，你們就像沙漠綠洲、久旱甘霖般滋養著學弟妹們。紹展、卓諭、餃妹、狗狗、宣融、組偉、小尻、佑先，很開心這段時間大家的相伴，一起學習和討論，互相取笑和打鬧，人家常說志同道合的夥伴最是難得。希望大家離開實驗室之後，各自發展宏圖，理想與現實合而為一，多年之後能光耀實驗室門楣。還有在職班的學長們，志銘學長、其昌學長和書賢學長，在我探路職場能給我一些經驗談，使我對漫漫前路有一點方向，不會那麼徬徨無助。

最後我想感謝自己的家人，因為研究繁忙，總是無法常回家，沒辦法好好的陪伴在你們身旁，有時候也不常打電話回去。反到是你們時常的關心，讓我身處遠離家鄉也有家鄉的溫暖。從襁褓到成熟的成年人了，人生一切都是由家裡提供養分讓我茁壯，謝謝你們。

Contents

Chapter 1 Introduction

1.1 Literature Review-----	1
1.2 Contributions-----	2

Chapter 2 Crossover Coupler Design using Asymmetric Branch-Line Hybrids

2.1 Crossover Coupler Design-----	4
2.1.1 Asymmetric Branch-Line Hybrid with Arbitrary Termination Impedances-----	5
2.1.2 Two Asymmetric Branch-Line Hybrids in a Cascade-----	6
2.2 Circuit Bandwidth-----	8
2.2.1 Block $ABCD$ matrix for Four-Port Network-----	8
2.2.2 Conversion between the Block $ABCD$ matrix and the 4×4 Y matrix-----	10
2.2.3 Bandwidth Calculation-----	15
2.3 Simulation and Measurement-----	27

Chapter 3 Dual-Band Crossover Coupler Design

3.1 Elementary Two-Port Network for Dual-Band Operation-----	32
3.2 Simulation and Measurement-----	35

Chapter 4 Conclusion

Conclusion-----	40
-----------------	----

Reference-----	41
----------------	----

List of Figures

Figure 2.1	Circuit schematic of an asymmetric branch-line hybrid.-----	5
Figure 2.2	(a) Proposed crossover coupler with arbitrary diagonal termination impedances.	
	(b) Analysis of (a) by the transmission line model.-----	7
Figure 2.3	(a) Voltage and current definitions in Z - and Y -parameter formulations.	
	(b) Voltage and current definitions in block $ABCD$ parameter formulations.-----	9
Figure 2.4	Block $ABCD$ matrices for analysis of a cascade of two four-ports.-----	10
Figure 2.5	Circuit schematic of a four port coupler.-----	17
Figure 2.6	Bandwidths measured by S -parameter responses. Port 1 and port 3 are terminated in Z_{01} and port 2 and port 4 are terminated in Z_{02} . $Z_{i1} = Z_{i2} = Z_{01}$. Curves 1 ~ 5 have $Z_{01}:Z_{02} = 1:1, 1:2, 1:4, 2:1, \text{ and } 4:1$, respectively. (a) $ S_{11} $ and $ S_{33} $. (b) $ S_{21} $ and $ S_{34} $. (c) $ S_{13} $ and $ S_{24} $. (d) $ S_{14} $ and $ S_{23} $. (e) $ S_{22} $ and $ S_{44} $.-----	20
Figure 2.7	Bandwidths measured by S -parameter responses. Port 1 and port 3 are terminated in Z_{01} and port 2 and port 4 are terminated in Z_{02} . $Z_{i1} = Z_{i2} = Z_{02}$. Curves 1 ~ 5 have $Z_{01}:Z_{02} = 1:1, 1:2, 1:4, 2:1, \text{ and } 4:1$, respectively. (a) $ S_{11} $ and $ S_{33} $. (b) $ S_{21} $ and $ S_{34} $. (c) $ S_{13} $ and $ S_{24} $. (d) $ S_{14} $ and $ S_{23} $. (e) $ S_{22} $ and $ S_{44} $.-----	23

Figure 2.8 Bandwidths measured by S -parameter responses. Port 1 and port 3 are terminated in Z_{01} and port 2 and port 4 are terminated in Z_{02} . $Z_{i1} = Z_{i2} = \sqrt{Z_{01}Z_{02}}$. Curves 1 ~ 5 have $Z_{01}:Z_{02} = 1:1, 1:2, 1:4, 2:1, \text{ and } 4:1$, respectively. (a) $|S_{11}|$ and $|S_{33}|$. (b) $|S_{21}|$ and $|S_{34}|$. (c) $|S_{13}|$ and $|S_{24}|$. (d) $|S_{14}|$ and $|S_{23}|$. (e) $|S_{22}|$ and $|S_{44}|$.-----**26**

Figure 2.9 The S -parameters of the first fabricated circuit with $Z_{o1} = 25 \Omega$, $Z_{o2} = 100 \Omega$, $Z_i = 100\Omega$ and $\Theta = 46^\circ$. (a) $|S_{11}|, |S_{21}|, |S_{31}|, |S_{41}|$. (b) $|S_{22}|, |S_{23}|, |S_{33}|$. (c) $|S_{24}|, |S_{34}|, |S_{44}|$. (d) The circuit photo. $W_1 \sim W_7$ are 2.06, 0.48, 1.01, 1.1, 1.18, 0.43 and 2.19 mm. $L_1 \sim L_7$ are 11.06, 11.69, 11.42, 11.39, 11.35, 11.72 and 11.02 mm.-----**29**

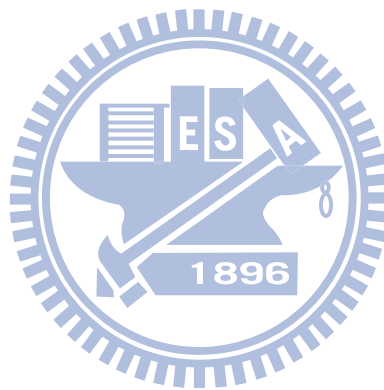
Figure 2.10 The S -parameters of the second fabricated circuit with $Z_{o1} = 100 \Omega$, $Z_{o2} = 50 \Omega$, $Z_i = 50 \Omega$ and $\Theta = 40^\circ$. (a) $|S_{11}|, |S_{21}|, |S_{31}|, |S_{41}|$. (b) $|S_{22}|, |S_{23}|, |S_{33}|$. (c) $|S_{24}|, |S_{34}|, |S_{44}|$. (d) Circuit photo. $W_1 \sim W_7$ are 1.33, 1.84, 0.74, 3.74, 0.26, 2.49 and 0.92 mm. $L_1 \sim L_7$ are 11.29, 11.12, 11.55, 10.7, 11.85, 10.95 and 11.47 mm.-----**31**

Figure 3.1 Two-port network for substituting a quarter-wave section.-----**34**

Figure 3.2 Design graphs for determining θ_{s1} and R . (a) $\theta_{s2} = 5^\circ$. (b) $\theta_{s2} = 10^\circ$. Both θ_{s1} and θ_{s2} values are referred to f_1 .-----**35**

Figure 3.3 Two cascaded asymmetric branch-line hybrids to form a new crossover coupler with arbitrary diagonal port impedances Z_{o1} and Z_{o2} .-----**36**

Figure 3.4 Simulation and measured responses of the fabricated dual-band crossover junction. (a) $|S_{11}|$ and $|S_{41}|$. (b) $|S_{21}|$ and $|S_{31}|$. (c) $|S_{22}|$ and $|S_{32}|$. (d) $|S_{12}|$ and $|S_{42}|$. $Z_{o1} = 50 \Omega$ and $Z_{o2} = 25 \Omega$. (e) Photograph of the experimental circuit.-----**39**

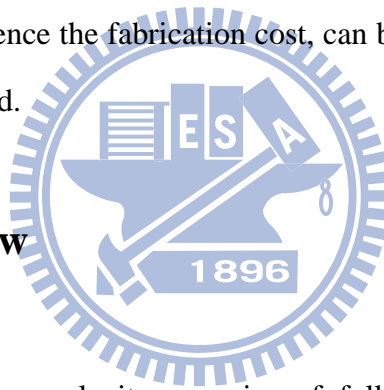


Chapter 1

Introduction

Crossover is an essential device for microwave and radio frequency integrated circuits. In a microstrip circuit [1], an air-bridge interconnect is an intuitive solution, and this three-dimensional structure exhibits a low-pass characteristic. In [2], two signal traces are laid on different metal layers and an additional grounded plane is placed in between to shield one signal from the other. One can expect that extra vias are required to have all the input and output terminals of the crossover in one metal plane. Obviously, if a fully planar crossover coupler can be realized with ideal transmission loss, return loss and isolation, not only the vias mentioned above and hence the fabrication cost, can be saved, but also the overall circuit performance can be enhanced.

1.1 Literature Review



To reduce the design complexity, a series of fully planar multi-port couplers with crossover applications have been investigated in [3-9]. Ideally, the crossover junction is supposed to provide 0-dB insertion loss to diagonal ports and perfect isolation to adjacent ports. In [3], microstrip and stripline crossovers are contrived on the basis of two cascaded branch-line hybrids. In [4], octave-wide matched symmetrical and reciprocal four- and five-port networks are proposed. A circular disk can also be designed as a symmetrical and reciprocal four-port crossover junction [5]. In [6], a novel planar configuration of 0-dB directional coupler is presented as a single-layer crossover in microwave integrated circuits. The circuit configured in a “window”-shape [7] may have an improved bandwidth if the characteristic impedances of the constitution branches can be properly designed. Recently, in [8-9], a double-ring structure is proposed for design of microstrip four-port crossover coupler.

The eigenmode model is developed for analysis to investigate the circuit performance. The measured data of the circuit show that the isolation and return loss of the prototype coupler exceed 20 dB over a bandwidth of 20%. In [10], a four-port crossover coupler with a simpler configuration is proposed and investigated.

Recent rapid progress in wireless communication systems has created a need of dual-band operation for RF devices [13-19]. In [13], a rigorous design is presented for microstrip bandpass filters with a dual-passband response in parallel-coupled and vertical-stacked configurations. In [14], a novel branch-line coupler is proposed to operate at two arbitrary frequencies with additional stubs. In [15], a two-port consisting of a stepped-impedance section with open stubs attached to its two ends is proposed to imitate the 90°-section at the two designated frequencies with different characteristic impedances. In [16], novel arbitrary dual-band microwave components based on components using right/left hand transmission lines have been presented. In [17], a novel elementary two-section impedance transformer has been shown to be capable of dual-band operation under unrestricted load and frequency conditions. In [18], a new dual-band 3 dB three-port power divider based on a two-section transmission-line transformer for arbitrary impedance terminations is proposed. In [19], two novel PIFA-related dual-band antennas with spiraled and coupled structures have been proposed and demonstrated. Note that all crossover junctions in [1]-[10] are designed to have identical diagonal port impedances and operate in a single passband. Thus, this thesis studies the dual-band design of the crossover junction based on the approach employed in [15]. Design graph will be provided.

1.2 Contribution

Crossover coupler can also be designed using two branch-line hybrids in a cascade [3]. By applying standard hybrid analysis techniques, theoretically, the signal emerges only at the

diagonal port of the composite structure, with no insertion loss, and no power emerges from the remaining two ports such that high isolation between two crossing signal channels can be achieved. Nevertheless, the design is limited to that the two crossover traces have identical characteristic impedances. Chapter 2 extends the realization of planar crossover coupler of which the two crossover signal traces are allowed to have different characteristic impedances. The circuit consists of two asymmetric branch-line hybrids [11-12] in cascade. Each hybrid is designed to have arbitrary power division and termination impedances. By properly selecting the structure parameters of each hybrid, a crossover coupler could be readily fulfilled. Measured results of a fabricated circuit agree very well with the simulated counterparts.

In Chapter 3, the design of crossover junction with unequal port impedances in Chapter 2 is extended to have a dual-band characteristic based on the approach in [16]. According to the best of our knowledge, this is the first dual-band crossover coupler in open literature, so that its performance deserves investigation. An experimental microstrip dual-band crossover coupler is simulated and measured for demonstration.

Chapter 4 draws the conclusion of this work.

Chapter 2

Crossover Coupler Design using Asymmetric Branch-Line Hybrids

Crossover coupler is one of the solutions to the problem that two transmission lines cross each other. It enables the two signal paths to have as low as interference with each other. This chapter presents a crossover coupler design based on two asymmetric branch-line hybrids with arbitrary power divisions in a cascade. It is a new idea to design a four-port crossover junction with different termination impedances. Block $ABCD$ matrix formulation is applied to the circuit to estimate the bandwidth. The relation between power division ratio of asymmetric branch-line hybrids and performance of the crossover coupler is also investigated.

2.1 Crossover Coupler Design

A crossover coupler can be designed using two branch-line hybrids in a cascade [3]. By applying standard hybrid analysis techniques, theoretically, the signal emerges only at the diagonal port of the composite structure, with no insertion loss, and no power emerges from the remaining two ports so that high isolation between two crossing signal channels can be achieved. Nevertheless, the design has hitherto been limited to that the two crossover traces have identical characteristic impedances. This Chapter extends the realization of planar crossover coupler of which the two crossover signal traces are allowed to have different characteristic impedances. The circuit consists of two asymmetric branch-line hybrids [12-13] in cascade. Each hybrid is designed to have arbitrary power division and termination impedances. By properly selecting the structure parameters of each hybrid, a crossover coupler can be readily fulfilled.

2.1.1 Asymmetric Branch-Line Hybrid with Arbitrary Termination Impedances

In [11-12], an asymmetric branch-line coupler with arbitrary termination impedance and arbitrary power division is proposed. Figure 2.1 shows this four port coupler terminated in arbitrary impedances Z_a , Z_b , Z_c and Z_d . It consists of four $\lambda/4$ -sections which form a ring. The impedances of four $\lambda/4$ -sections are Z_1 , Z_2 , Z_3 and Z_4 . When power is fed into port 1, phase difference of the two output waves at port 2 and port 3 is 90° . The ratio $|S_{21}|/|S_{31}|$ is d_1/d_2 while port 4 is isolated. The design equations are as follows. For $Z_a = Z_b = Z_c = Z_d$ and $d_1 = d_2$, the result is the well-known conventional branch-line coupler [3].

$$Z_1 = \sqrt{\frac{d_1^2}{d_1^2 + d_2^2}} \sqrt{Z_a Z_b} \quad (2.1a)$$

$$Z_2 = \frac{d_1}{d_2} \sqrt{Z_b Z_c} \quad (2.1b)$$

$$Z_3 = \sqrt{\frac{d_1^2}{d_1^2 + d_2^2}} \sqrt{Z_c Z_d} \quad (2.1c)$$

$$Z_4 = \frac{d_1}{d_2} \sqrt{Z_d Z_a} \quad (2.1d)$$

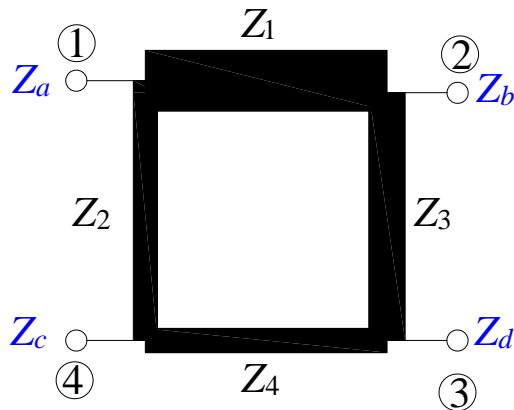


Figure 2.1 Circuit schematic of an asymmetric branch-line hybrid.

2.1.2 Two Asymmetric Branch-Line Hybrids in a Cascade

Figure 2.2(a) shows the schematic of the proposed crossover coupler. It consists of seven quarter-wavelength sections with characteristic impedances $Z_1 \sim Z_7$. The termination impedances of the two pairs of the diagonal ports are Z_{o1} and Z_{o2} . The circuit can be treated as two cascaded asymmetric branch-line hybrids as shown in Figure 2.2(b). Each hybrid possesses arbitrary power division and termination impedances. For impedance matching purpose, the two output terminations of the first hybrid, Z_{i1} and Z_{i2} , are designed to be the same as the two input counterparts of the second circuit. Since the sections Z_{a3} and Z_{b2} are in shunt connection, we have $Z_4 = Z_{a3} // Z_{b2}$. For coupler i ($i = 1, 2$) at the center frequency, let the outputs at their individual through and coupled ports be designated as $-j\alpha_i$ and $-\beta_i$, respectively. Here, α_i and β_i are positive real numbers satisfying $\alpha_i^2 + \beta_i^2 = 1$. Applying the standard hybrid analysis technique, we have

$$S_{21} = (-j\alpha_1)(-j\alpha_2) + (-\beta_1)(-\beta_2) = -\alpha_1\alpha_2 + \beta_1\beta_2 \quad (2.2a)$$

$$S_{31} = (-j\alpha_1)(-\beta_2) + (-\beta_1)(-j\alpha_2) = j(\alpha_1\beta_2 + \beta_1\alpha_2) \quad (2.2b)$$

Note that the design specifications require that $|S_{11}| = |S_{21}| = |S_{41}| = 0$ and $|S_{31}| = 1$. After some algebraic manipulation, it can be validated that $\alpha_1 = \beta_2$ and $\beta_1 = \alpha_2$. By employing the design equations in [3] and [12], the characteristic impedances of the branch-line sections can be written as

$$Z_{a1} = \sqrt{Z_{o1}Z_{i1}} \sin \Theta \quad (2.3a)$$

$$Z_{a2} = \sqrt{Z_{o1}Z_{o2}} \tan \Theta \quad (2.3b)$$

$$Z_{a3} = \sqrt{Z_{i1}Z_{i2}} \tan \Theta \quad (2.3c)$$

$$Z_{a4} = \sqrt{Z_{i2}Z_{o2}} \sin \Theta \quad (2.3d)$$

$$Z_{b1} = \sqrt{Z_{o2}Z_{i1}} \cos \Theta \quad (2.4a)$$

$$Z_{b2} = \sqrt{Z_{i1}Z_{i2}} \cot \Theta \quad (2.4b)$$

$$Z_{b3} = \sqrt{Z_{o1}Z_{o2}} \cot \Theta \quad (2.4c)$$

$$Z_{b4} = \sqrt{Z_{i2}Z_{o1}} \cos \Theta \quad (2.4d)$$

where $\sin \Theta = \alpha_1$ and $\cos \Theta = \beta_1$. From (2.3) and (2.4), provided that Z_{o1} and Z_{o2} are known, Z_{ak} and Z_{bk} ($k = 1, 2, 3$ and 4) can be readily obtained once Θ , Z_{i1} and Z_{i2} are given. Consequently, there are several degrees of freedom for the design since Θ , Z_{i1} and Z_{i2} can be arbitrary. The only concern for choosing their values should be the realization of the line widths of the fabrication process.

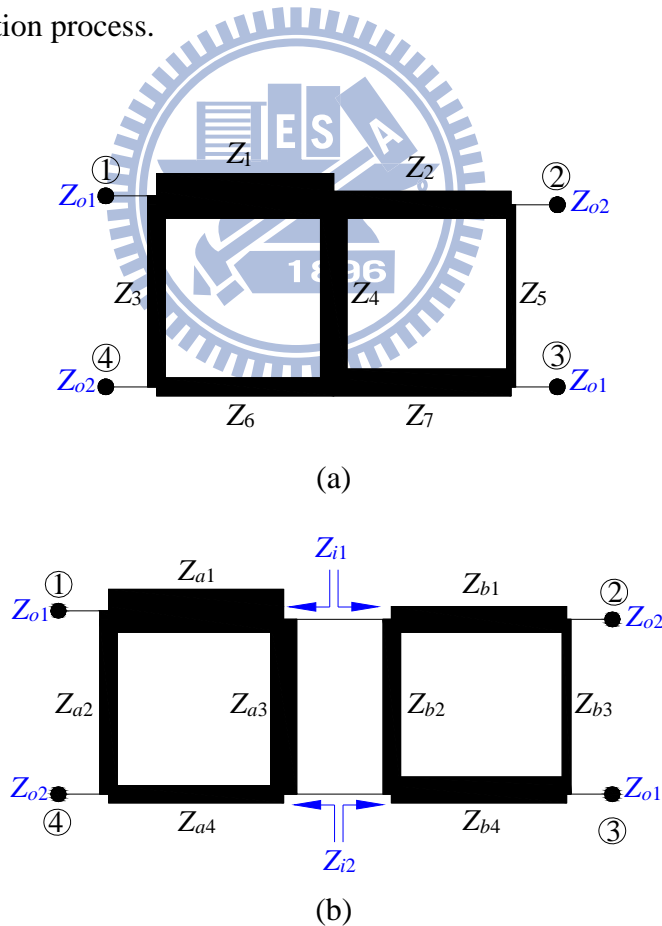


Figure 2.2 (a) Proposed crossover coupler with arbitrary diagonal termination impedances. (b) Analysis of (a) by the transmission line model.

2.2 Circuit Bandwidth

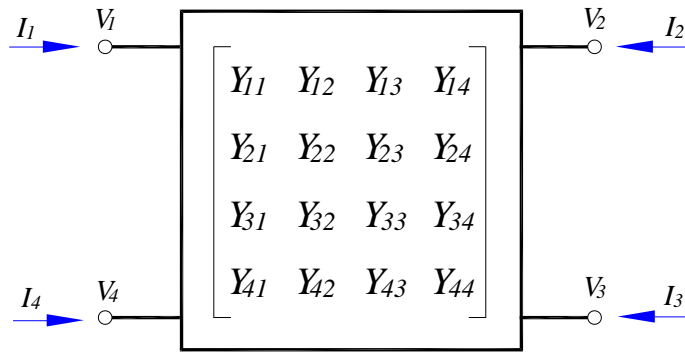
2.2.1 Block *ABCD* Matrix for Four-Port Network

In Figure 2.3 (a) and (b), port voltages and currents are defined at various terminals of a four-port network for *Y*-, *Z*- and *ABCD*-parameter analyses. Admittance and impedance matrices are used to describe the relation between the port voltages and currents in Figure 2.3 (a). The admittance matrix [*Y*] of the microwave network relates these voltages and currents as shown in (2.5):

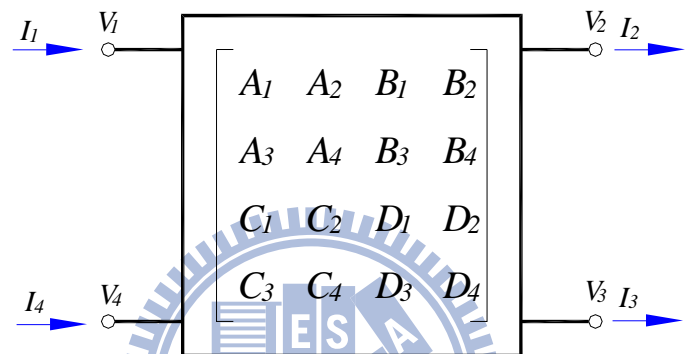
$$\begin{bmatrix} I_1 \\ I_2 \\ I_3 \\ I_4 \end{bmatrix} = \begin{bmatrix} Y_{11} & Y_{12} & Y_{13} & Y_{14} \\ Y_{21} & Y_{22} & Y_{23} & Y_{24} \\ Y_{31} & Y_{32} & Y_{33} & Y_{34} \\ Y_{41} & Y_{42} & Y_{43} & Y_{44} \end{bmatrix} \begin{bmatrix} V_1 \\ V_2 \\ V_3 \\ V_4 \end{bmatrix} \equiv [Y] \begin{bmatrix} V_1 \\ V_2 \\ V_3 \\ V_4 \end{bmatrix} \quad (2.5)$$

The impedance matrix can be defined in a similar fashion. The matrices [*Y*] and [*Z*] can be used to characterize a microwave network, but in practice when a microwave network consists of a cascade of two or more four-port networks, it is convenient to use a 4-by-4 *ABCD*-parameter for analysis purpose. The *ABCD* matrix of the cascade of two or more four-port can be easily obtained by directly multiplying the *ABCD* matrices of the each four-port, as shown in Figure 2.4. Mathematically, the voltages and currents of the two ports on the left hand side of the network are related to those on the right hand side by (2.6):

$$\begin{bmatrix} V_1 \\ V_4 \\ I_1 \\ I_4 \end{bmatrix} = \begin{bmatrix} A_1 & A_2 & B_1 & B_2 \\ A_3 & A_4 & B_3 & B_4 \\ C_1 & C_2 & D_1 & D_2 \\ C_3 & C_4 & D_3 & D_4 \end{bmatrix} \begin{bmatrix} V_2 \\ V_3 \\ I_2 \\ I_3 \end{bmatrix} \quad (2.6)$$



(a)



(b)

Figure 2.3 (a) Voltage and current definitions in Z- and Y-parameter formulations. (b) Voltage and current definitions in block $ABCD$ parameter formulations.

For the voltages and currents of a four-port in the block $ABCD$ -parameter formulation shown in Figure 2.3 (b), the directions of currents at port 2 and port 3 are opposite to those in the Y - and Z -parameter formulation. By using similar definition for the traditional two-port $ABCD$ matrix, each of the A_i -entries in block $ABCD$ can be determined by applying input voltages at port 1 and port 4, and measuring the open-circuit output voltages at port 2 and port 3. Similarly, each entry in block B is the ratio of input voltages to short-circuit output currents, those in block C is the ratio of input currents to open-circuit output voltages, and those in block D is the ratio of input currents to short-circuit currents. Detailed derivations are given in the following subsections.

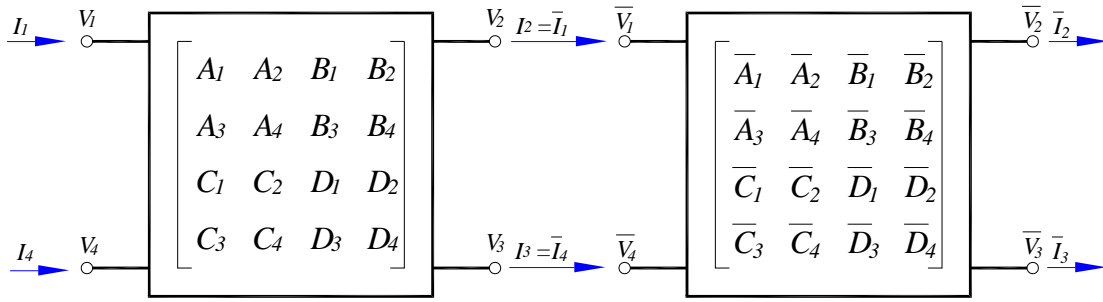


Figure 2.4 Block $ABCD$ matrices for analysis of a cascade of two four-ports.

2.2.2 Conversion between the Block $ABCD$ Matrix and the 4×4 Y Matrix

From (2.6), we have

$$A_1 = \left. \frac{V_1}{V_2} \right|_{V_3=0, I_2=0, I_3=0} \quad (2.7)$$

Substituting $V_3 = 0$, $I_2 = 0$ and $I_3 = 0$ into the relation of voltages and currents in the Y matrices, we have

$$I_2 = Y_{21}V_1 + Y_{22}V_2 + Y_{24}V_4 = 0 \quad (2.8a)$$

$$I_3 = Y_{31}V_1 + Y_{32}V_2 + Y_{34}V_4 = 0 \quad (2.8b)$$

Multiplying (2.8a) by Y_{34} and subtracting (2.8b) multiplied by Y_{24} from it, we can eliminate V_4 and obtain the relation between V_1 and V_2 . Then the transformation of Y -parameters to A_1 can be derived as shown in (2.9a). All other elements of block A can also be derived similarly and are given in (2.9b) ~ (2.9d).

$$A_1 = \frac{Y_{32}Y_{24} - Y_{22}Y_{34}}{Y_{21}Y_{34} - Y_{31}Y_{24}} \quad (2.9a)$$

$$A_2 = \frac{Y_{33}Y_{24} - Y_{23}Y_{34}}{Y_{21}Y_{34} - Y_{31}Y_{24}} \quad (2.9b)$$

$$A_3 = \frac{Y_{22}Y_{31} - Y_{32}Y_{21}}{Y_{21}Y_{34} - Y_{31}Y_{24}} \quad (2.9c)$$

$$A_4 = \frac{Y_{23}Y_{31} - Y_{33}Y_{21}}{Y_{21}Y_{34} - Y_{31}Y_{24}} \quad (2.9d)$$

From (2.6), B_1 of block B is defined as

$$B_1 = \frac{V_1}{I_2} \Big|_{V_2=0, V_3=0, I_3=0} \quad (2.10)$$

According to the relation of voltages and currents in the Y -matrix, the following equations can be derived with $V_2 = 0$, $V_3 = 0$ and $I_3 = 0$:

$$I_3 = Y_{31}V_1 + Y_{34}V_4 = 0 \quad (2.11a)$$

$$-I_2 = Y_{21}V_1 + Y_{24}V_4 \quad (2.11b)$$

Note that the direction of I_2 in the Y -matrix is opposite to that in the block $ABCD$ matrices. The relation of V_1 and V_4 in (2.11a) is used in (2.11b). Then, the ratio V_1/I_2 can be derived as shown in (2.12a). Similarly, all other elements block B can be obtained as follows:

$$B_1 = \frac{-Y_{34}}{Y_{21}Y_{34} - Y_{31}Y_{24}} \quad (2.12a)$$

$$B_2 = \frac{Y_{24}}{Y_{21}Y_{34} - Y_{31}Y_{24}} \quad (2.12b)$$

$$B_3 = \frac{Y_{31}}{Y_{21}Y_{34} - Y_{31}Y_{24}} \quad (2.12c)$$

$$B_4 = \frac{-Y_{21}}{Y_{21}Y_{34} - Y_{31}Y_{24}} \quad (2.12d)$$

From (2.6), C_1 of block C is defined as

$$C_1 = \frac{I_1}{V_2} \Big|_{V_3=0, I_2=0, I_3=0} \quad (2.13)$$

According to the relation of voltages and currents in the Y -matrix and the conditions $V_3 = 0$, $I_2 = 0$ and $I_3 = 0$, the following equations can be derived:

$$I_2 = Y_{21}V_1 + Y_{22}V_2 + Y_{24}V_4 = 0 \quad (2.14a)$$

$$I_3 = Y_{31}V_1 + Y_{32}V_2 + Y_{34}V_4 = 0 \quad (2.14b)$$

$$I_1 = Y_{11}V_1 + Y_{12}V_2 + Y_{14}V_4 \quad (2.14c)$$

(2.14a) and (2.14b) can be used to eliminate V_4 and express V_1 as a function of V_2 . Similarly, V_4 can be expressed as a function of V_2 . Applying these relations to (2.14c) can eliminate V_1 and V_2 . Then, the ratio of I_1/V_2 can be obtained as shown in (2.15a). All other elements of block C can also be derived as shown in (2.15b) ~ (2.15d):

$$C_1 = \frac{Y_{11}(Y_{32}Y_{24} - Y_{22}Y_{34}) + Y_{14}(Y_{22}Y_{31} - Y_{32}Y_{21})}{Y_{21}Y_{34} - Y_{31}Y_{24}} + Y_{12} \quad (2.15a)$$

$$C_2 = -\frac{Y_{11}(Y_{34}Y_{23} - Y_{24}Y_{33}) + Y_{14}(Y_{21}Y_{33} - Y_{31}Y_{23})}{Y_{21}Y_{34} - Y_{31}Y_{24}} + Y_{13} \quad (2.15b)$$

$$C_3 = \frac{Y_{41}(Y_{32}Y_{24} - Y_{22}Y_{34}) + Y_{44}(Y_{22}Y_{31} - Y_{32}Y_{21})}{Y_{21}Y_{34} - Y_{31}Y_{24}} + Y_{42} \quad (2.15c)$$

$$C_4 = -\frac{Y_{41}(Y_{34}Y_{23} - Y_{24}Y_{33}) + Y_{44}(Y_{21}Y_{33} - Y_{31}Y_{23})}{Y_{21}Y_{34} - Y_{31}Y_{24}} + Y_{43} \quad (2.15d)$$

From (2.6), D_1 of block D is defined as

$$D_1 = \frac{I_1}{I_2} \Big|_{V_2=0, V_3=0, I_3=0} \quad (2.16)$$

The relations in the Y matrices with the conditions $V_2 = 0$, $V_3 = 0$ and $I_3 = 0$ are used. Then, the following equations can be obtained.

$$I_3 = Y_{31}V_1 + Y_{34}V_4 = 0 \quad (2.17a)$$

$$I_1 = Y_{11}V_1 + Y_{14}V_4 \quad (2.17b)$$

$$-I_2 = Y_{21}V_1 + Y_{24}V_4 \quad (2.17c)$$

From (2.17a) V_4 can be written as a function of V_1 . Substituting this function into (2.17a) and (2.17b), the ratio I_1/I_2 in (2.16) can be obtained. D_2 , D_3 and D_4 can be derived in a similar way:

$$D_1 = \frac{Y_{31}Y_{14} - Y_{11}Y_{34}}{Y_{21}Y_{34} - Y_{31}Y_{24}} \quad (2.18a)$$

$$D_2 = \frac{Y_{24}Y_{11} - Y_{21}Y_{14}}{Y_{21}Y_{34} - Y_{31}Y_{24}} \quad (2.18b)$$

$$D_3 = \frac{Y_{44}Y_{31} - Y_{41}Y_{34}}{Y_{21}Y_{34} - Y_{31}Y_{24}} \quad (2.18c)$$

$$D_4 = \frac{Y_{24}Y_{41} - Y_{21}Y_{44}}{Y_{21}Y_{34} - Y_{31}Y_{24}} \quad (2.18d)$$

Based the procedure shown above, the four-port Y -parameters can be readily transformed into block $ABCD$ parameters. Next, we will show the formulation for transforming $ABCD$ -parameters into Y -parameters for a four port network.

From (2.5),

$$Y_{11} = \frac{I_1}{V_1} \Big|_{V_2=0, V_3=0, V_4=0} \quad (2.19)$$

According to the definitions of the block $ABCD$ matrix, and the conditions $V_2 = 0$, $V_3 = 0$ and $V_4 = 0$, the following equations can be used to solve the ratio I_1/V_1 :

$$V_4 = -I_2 B_3 - I_3 B_4 = 0 \quad (2.20a)$$

$$I_1 = -I_2 D_1 - I_3 D_2 \quad (2.20b)$$

$$V_1 = -I_2 B_1 - I_3 B_2 \quad (2.20c)$$

After some algebraic operations, the result is

$$Y_{11} = \frac{D_1 B_4 - D_2 B_3}{B_1 B_4 - B_2 B_3} \quad (2.21a)$$

All other elements in the Y -matrix can be obtained in a similar fashion:

$$Y_{14} = \frac{B_1 D_2 - B_2 D_1}{B_1 B_4 - B_2 B_3} \quad (2.21b)$$

$$Y_{41} = \frac{B_4 D_3 - B_3 D_4}{B_1 B_4 - B_2 B_3} \quad (2.21c)$$

$$Y_{44} = \frac{B_2 D_3 - B_1 D_4}{B_1 B_4 - B_2 B_3} \quad (2.21d)$$

$$Y_{12} = \frac{D_1(A_3 B_2 - A_1 B_4) + D_2(A_1 B_3 - A_3 B_1)}{B_1 B_4 - B_2 B_3} + C_1 \quad (2.22a)$$

$$Y_{13} = \frac{D_1(A_4B_2 - A_2B_4) + D_2(A_2B_3 - A_4B_1)}{B_1B_4 - B_2B_3} + C_2 \quad (2.22b)$$

$$Y_{42} = \frac{D_3(A_3B_2 - A_1B_4) + D_4(A_1B_3 - A_3B_1)}{B_1B_4 - B_2B_3} + C_3 \quad (2.22c)$$

$$Y_{43} = \frac{D_3(A_4B_2 - A_2B_4) + D_4(A_2B_3 - A_4B_1)}{B_1B_4 - B_2B_3} + C_4 \quad (2.22d)$$

$$Y_{21} = \frac{-B_4}{B_1B_4 - B_2B_3} \quad (2.23a)$$

$$Y_{31} = \frac{B_3}{B_1B_4 - B_2B_3} \quad (2.23b)$$

$$Y_{24} = \frac{B_2}{B_1B_4 - B_2B_3} \quad (2.23c)$$

$$Y_{34} = \frac{-B_1}{B_1B_4 - B_2B_3} \quad (2.23d)$$

$$Y_{22} = \frac{A_1B_4 - A_3B_2}{B_1B_4 - B_2B_3} \quad (2.24a)$$

$$Y_{32} = \frac{A_3B_1 - A_1B_3}{B_1B_4 - B_2B_3} \quad (2.24b)$$

$$Y_{23} = \frac{A_2B_4 - A_4B_2}{B_1B_4 - B_2B_3} \quad (2.24c)$$

$$Y_{33} = \frac{A_4B_1 - A_2B_3}{B_1B_4 - B_2B_3} \quad (2.24d)$$

2.2.3 Bandwidth Calculation

Figure 2.5 shows a four-port coupler with arms of arbitrary lengths, arbitrary characteristic impedances and arbitrary terminations. Analysis of the crossover coupler in Figure 2.2 can be formulated by the block $ABCD$ matrices. To find the entries of the block $ABCD$ matrix, the Y -parameters of a four-port coupler in Figure 2.5 are derived first. By definition, $Y_{11} = I_1/V_1$ when port 2, 3 and 4 are short-circuited. Based on the input admittance of a loaded transmission line, the result is shown in (2.25a). All other entries in the Y -matrix can be obtained in a similar fashion, and the results are in (2.25b) to (2.25i).

$$Y_{11} = -jY_1 \cot \theta_1 - jY_2 \cot \theta_2 \quad (2.25a)$$

$$Y_{22} = -jY_1 \cot \theta_1 - jY_3 \cot \theta_3 \quad (2.25b)$$

$$Y_{33} = -jY_3 \cot \theta_3 - jY_4 \cot \theta_4 \quad (2.25c)$$

$$Y_{44} = -jY_2 \cot \theta_2 - jY_4 \cot \theta_4 \quad (2.25d)$$

$$Y_{12} = Y_{21} = jY_1 \csc \theta_1 \quad (2.25e)$$

$$Y_{14} = Y_{41} = jY_2 \csc \theta_2 \quad (2.25f)$$

$$Y_{23} = Y_{32} = jY_3 \csc \theta_3 \quad (2.25g)$$

$$Y_{34} = Y_{43} = jY_4 \csc \theta_4 \quad (2.25h)$$

$$Y_{13} = Y_{31} = Y_{24} = Y_{42} = 0 \quad (2.25i)$$

These Y -parameters are then transformed into four-port block $ABCD$ parameters as shown in section 2.2.2. Multiplying the $ABCD$ matrices of each stage, the total $ABCD$ matrix of the crossover in Figure 2.2 can be obtained. The overall S -parameter matrix can be calculated when the total $ABCD$ matrix is transformed into Y matrix which is then transformed into the S -matrix. If a 20-dB return loss, 0.5-dB insertion loss and 20-dB isolation are referred, the bandwidth of the crossover coupler can be obtained by computation using a computer program.

The proposed crossover coupler in Figure 2.2 has four design parameters Z_{o1} , Z_{o2} , $Z_i = Z_{i1} = Z_{i2}$ and Θ . When the above parameters are determined, the impedances of the arms $Z_1 \sim Z_7$ can be obtained from (2.3) and (2.4). Z_{o1} , Z_{o2} and Z_i are fixed and S -parameters are measured when port 1 and port 3 are terminated in Z_{o1} and port 2 and port 4 are terminated in Z_{o2} . The

values of Z_{01} and Z_{02} will not affect the S -parameters but the ratio of Z_{01} to Z_{02} does, because $Z_1 \sim Z_7$ will maintain the same ratio when the ratio of Z_{01} to Z_{02} is fixed. Then power division ratio Θ is swept, and the bandwidth is calculated. The relation between Θ and the calculated bandwidth are discussed as follows.

Figure 2.6 shows the calculated bandwidth for $Z_{i1} = Z_{i2} = Z_{01}$. Each S -parameter may have its own response and bandwidth. Figure 2.6 (a) shows the bandwidth of $|S_{11}|$ and $|S_{33}|$, Figure 2.6 (b) shows those of $|S_{12}|$ and $|S_{34}|$, Figure 2.6 (c) shows those of $|S_{13}|$ and $|S_{24}|$, Figure 2.6 (d) shows those of $|S_{14}|$ and $|S_{23}|$, and Figure 2.6 (e) shows those of $|S_{22}|$ and $|S_{44}|$. The other S -parameters can be known by the reciprocity theorem. In each port, curve 1 uses $Z_{01}:Z_{02} = 1:1$, curve 2 uses $Z_{01}:Z_{02} = 1:2$, curve 3 uses $Z_{01}:Z_{02} = 1:4$, curve 4 uses $Z_{01}:Z_{02} = 2:1$ and curve 5 uses $Z_{01}:Z_{02} = 4:1$. When $\Theta = 45^\circ$, the circuit has the best matching condition for all termination impedance ratios, while the circuit has the best isolation when the power coefficient is 20° or 70° . In Figure 2.7 and Figure 2.8, Z_{i1} and Z_{i2} are replaced by Z_{02} and $\sqrt{Z_{01}Z_{02}}$, respectively. The trend of the circuit bandwidths of the S -parameters is similar to those in Figure 2.7.

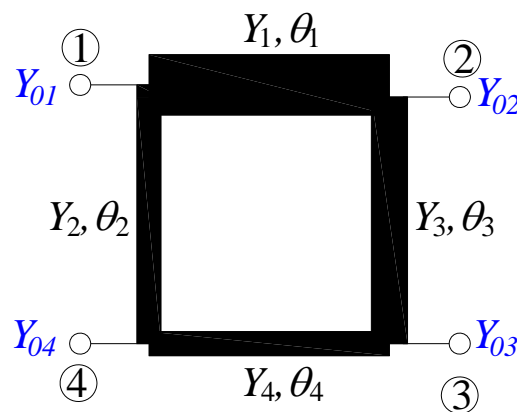
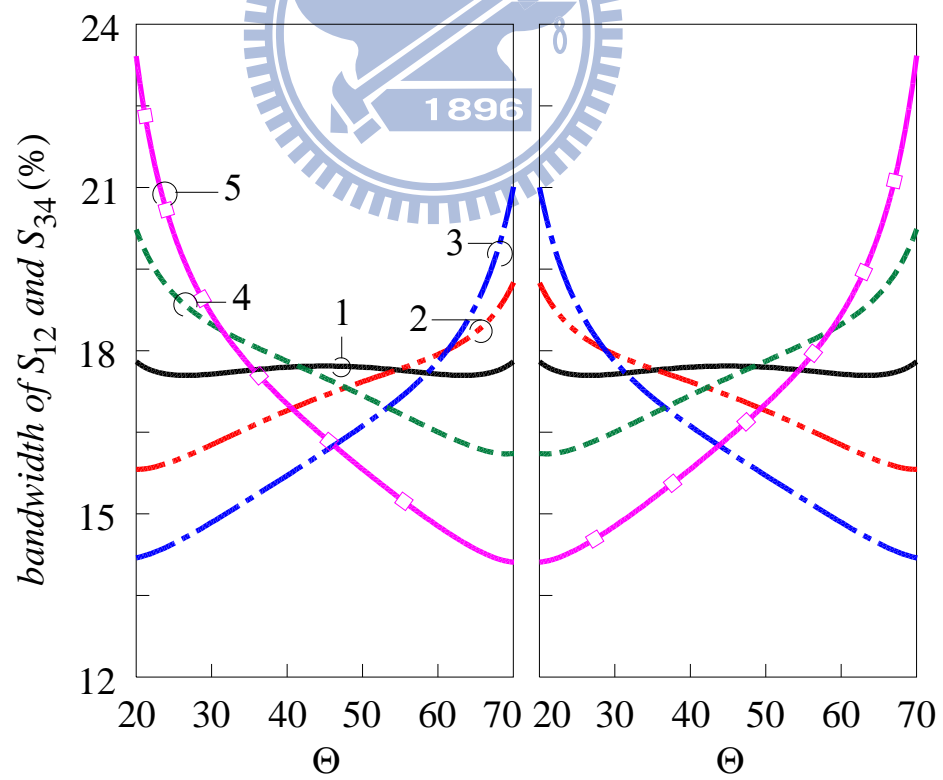
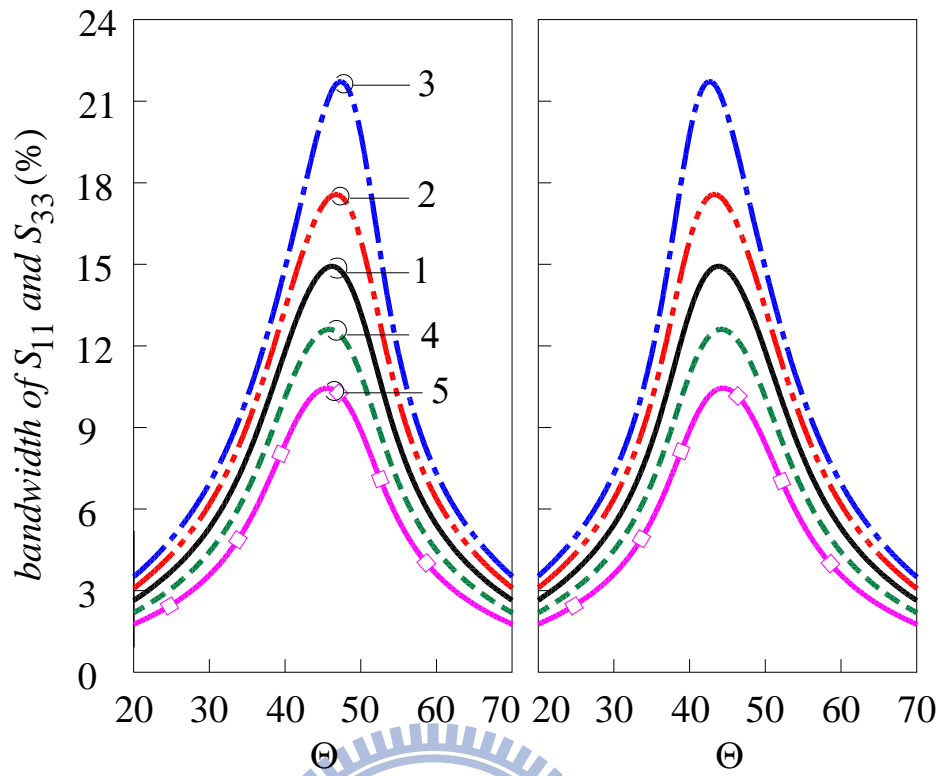
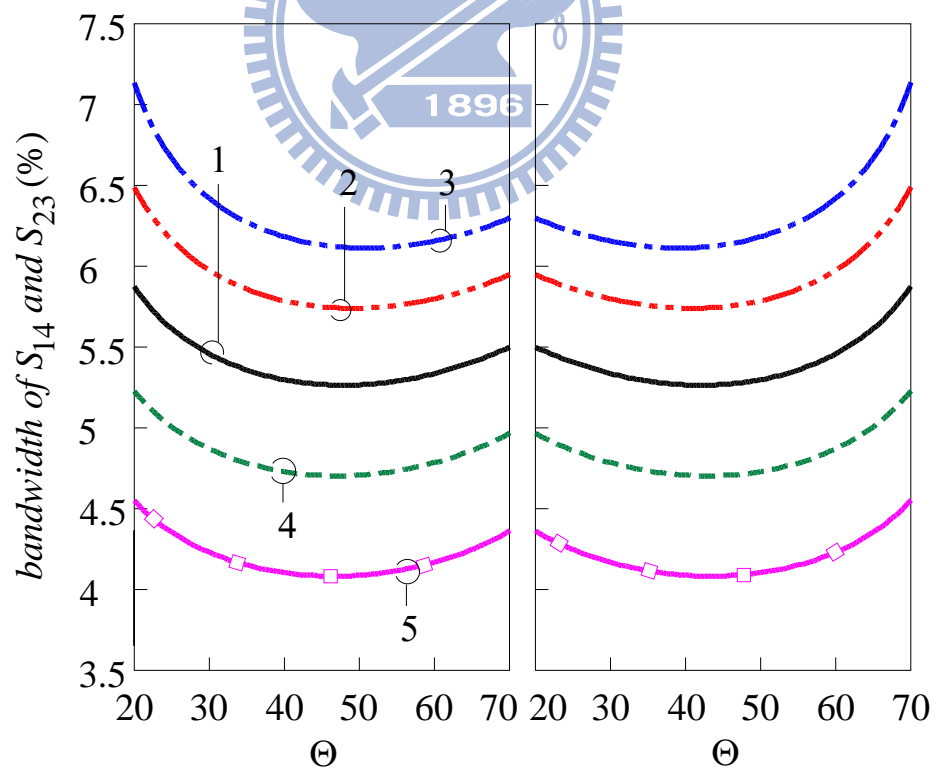
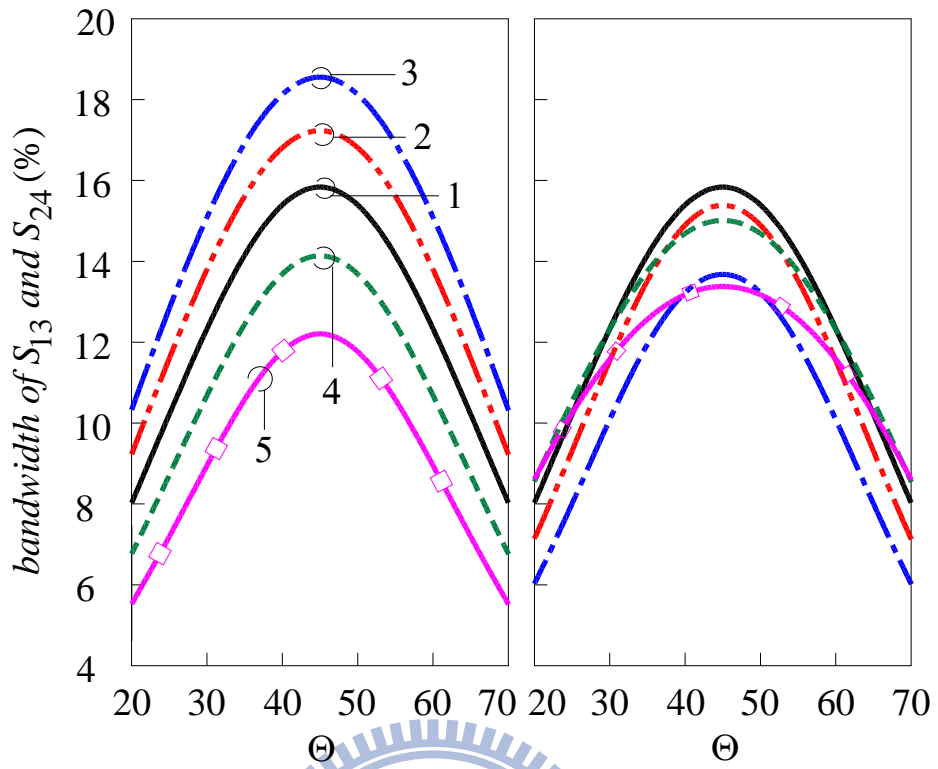


Figure 2.5 Circuit schematic of a four port coupler.



(b)



(d)

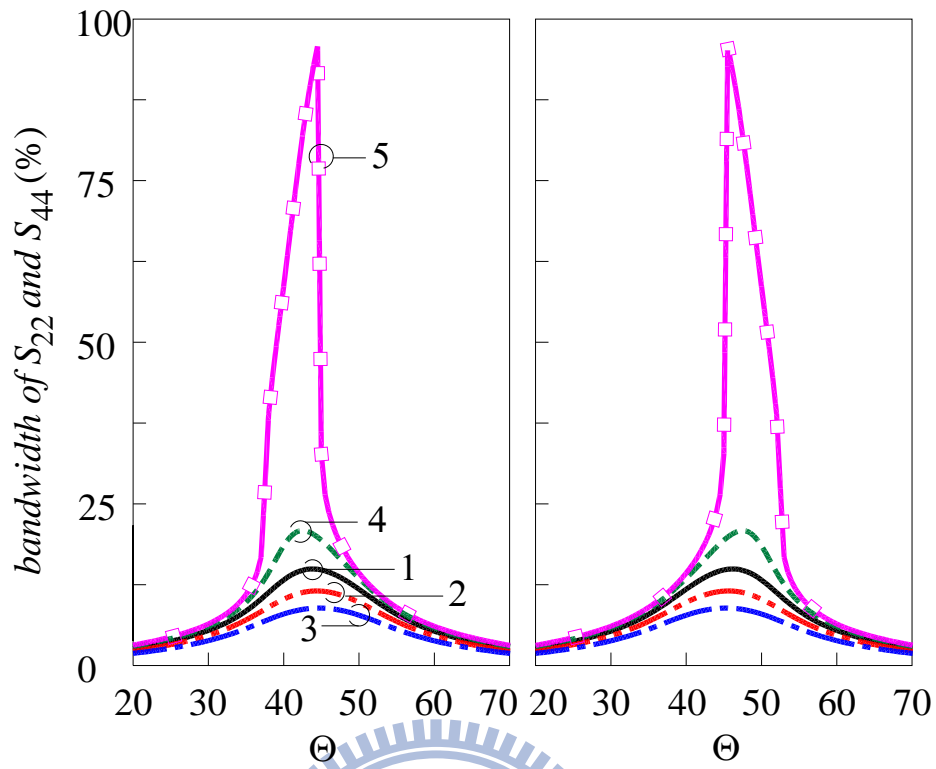
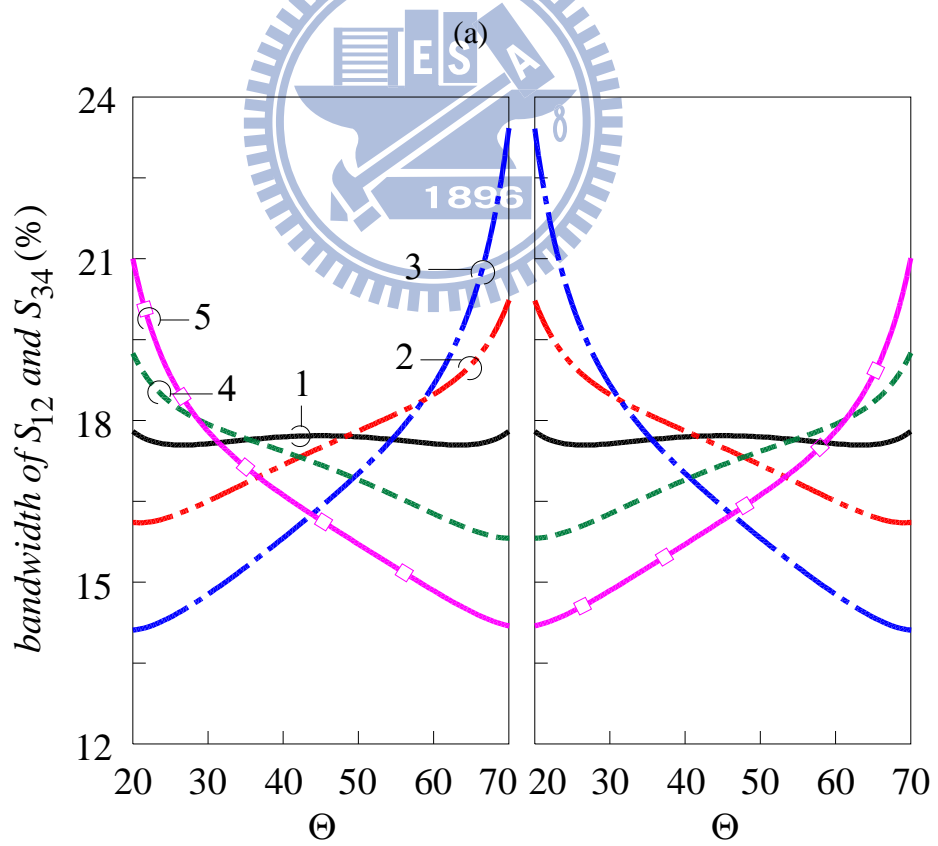
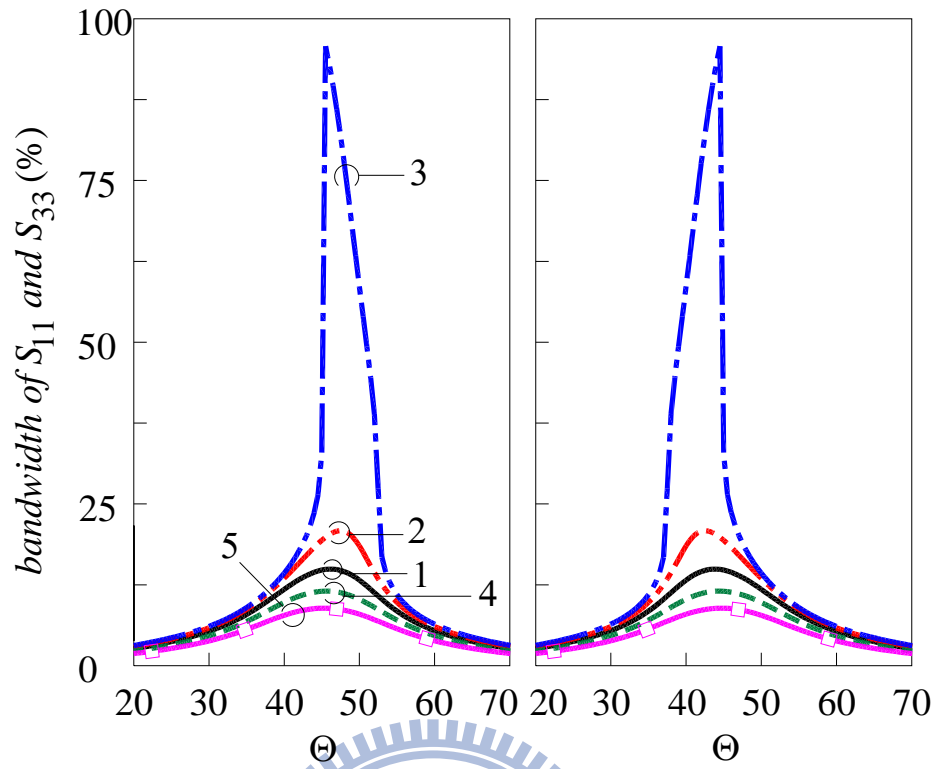
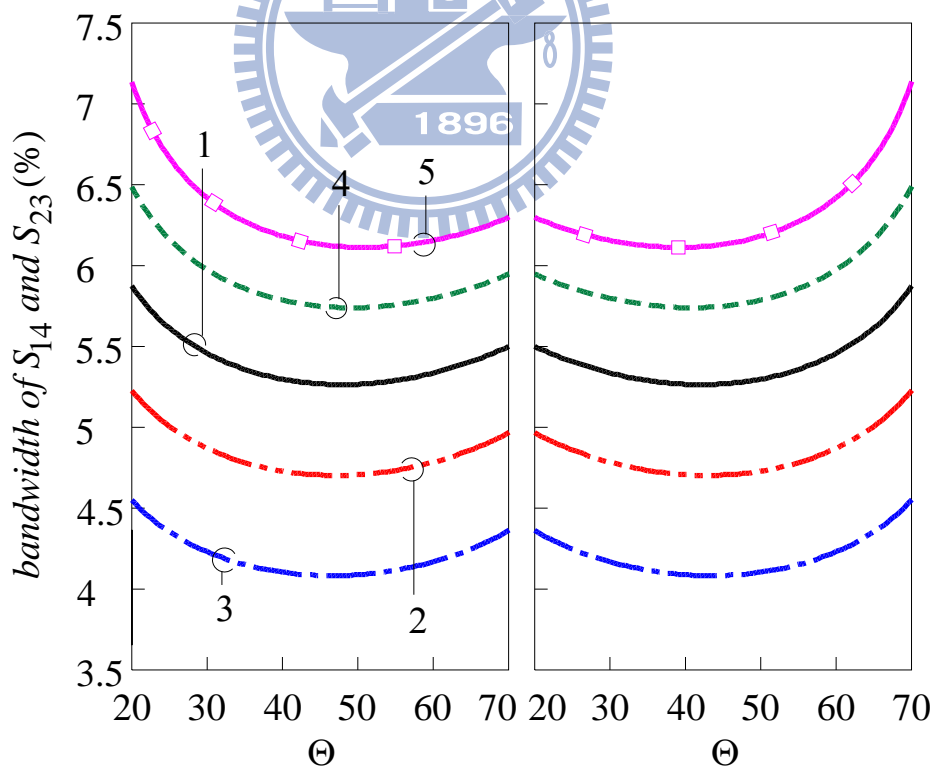
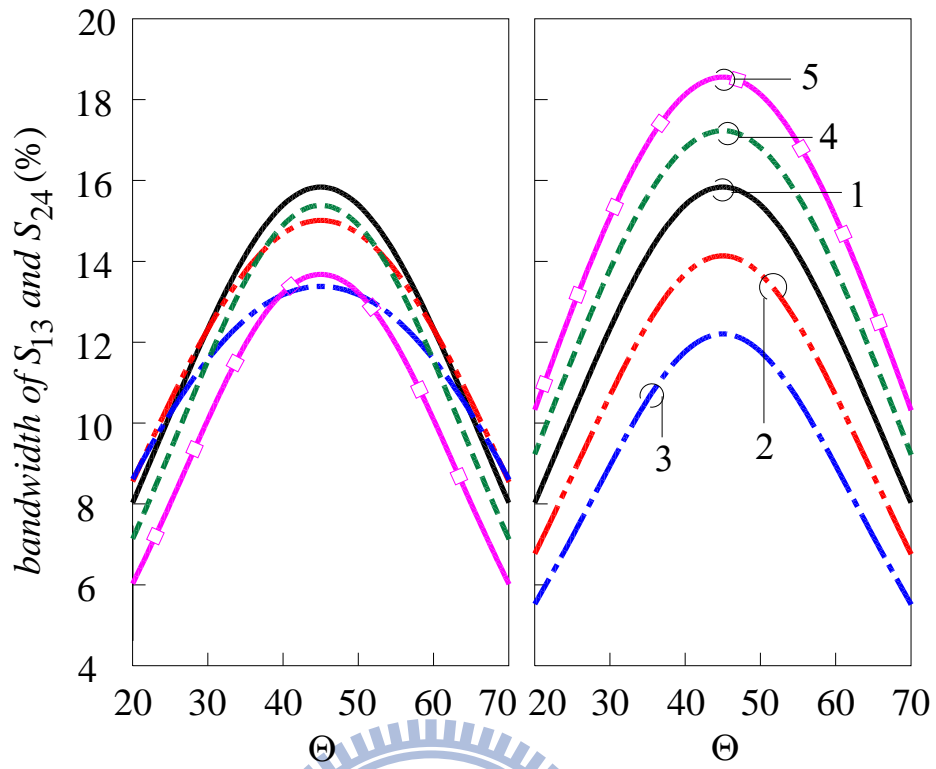


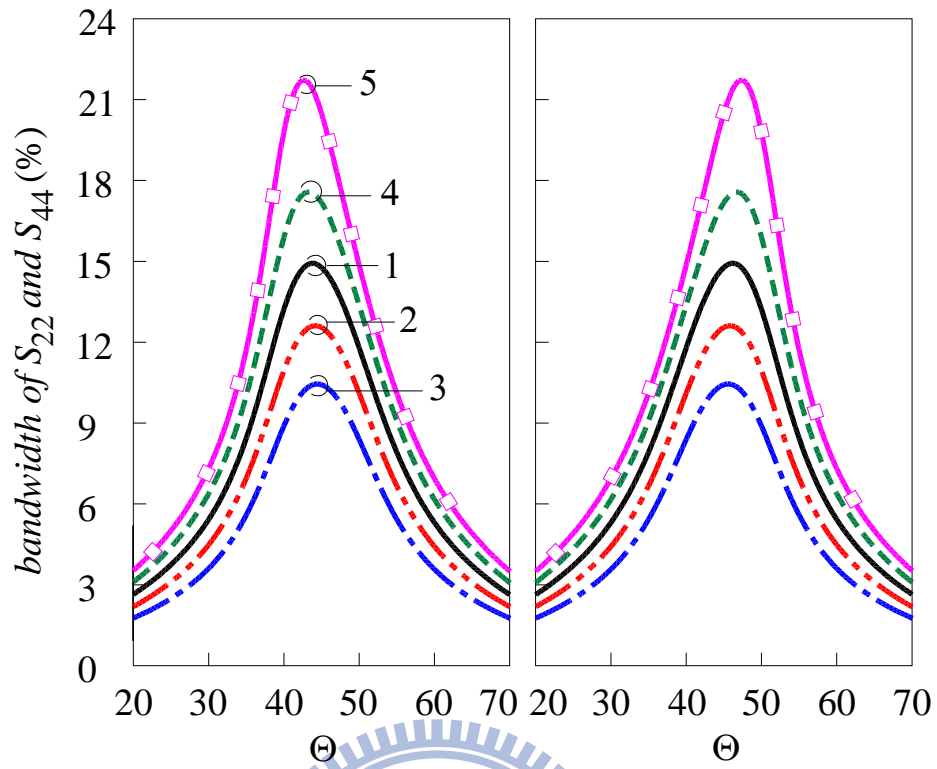
Figure 2.6 Bandwidths measured by S -parameter responses. Port 1 and port 3 are terminated in Z_{01} and port 2 and port 4 are terminated in Z_{02} . $Z_{i1} = Z_{i2} = Z_{01}$. Curves 1 ~ 5 have $Z_{01}:Z_{02} = 1:1, 1:2, 1:4, 2:1, \text{ and } 4:1$, respectively. (a) $|S_{11}|$ and $|S_{33}|$. (b) $|S_{21}|$ and $|S_{34}|$. (c) $|S_{13}|$ and $|S_{24}|$. (d) $|S_{14}|$ and $|S_{23}|$. (e) $|S_{22}|$ and $|S_{44}|$.



(b)

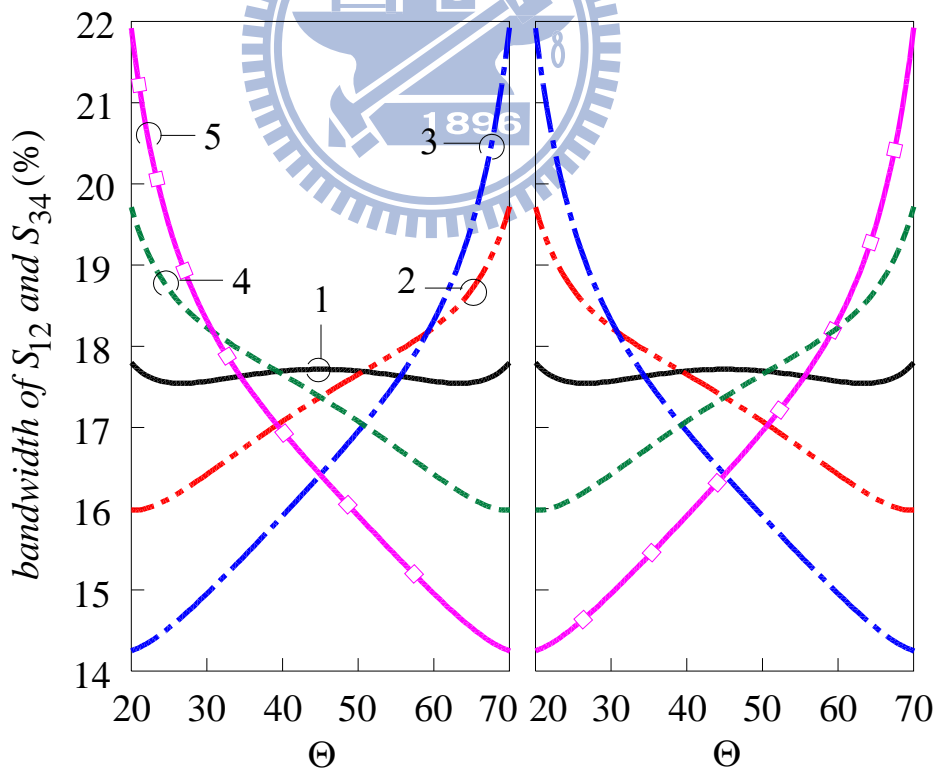
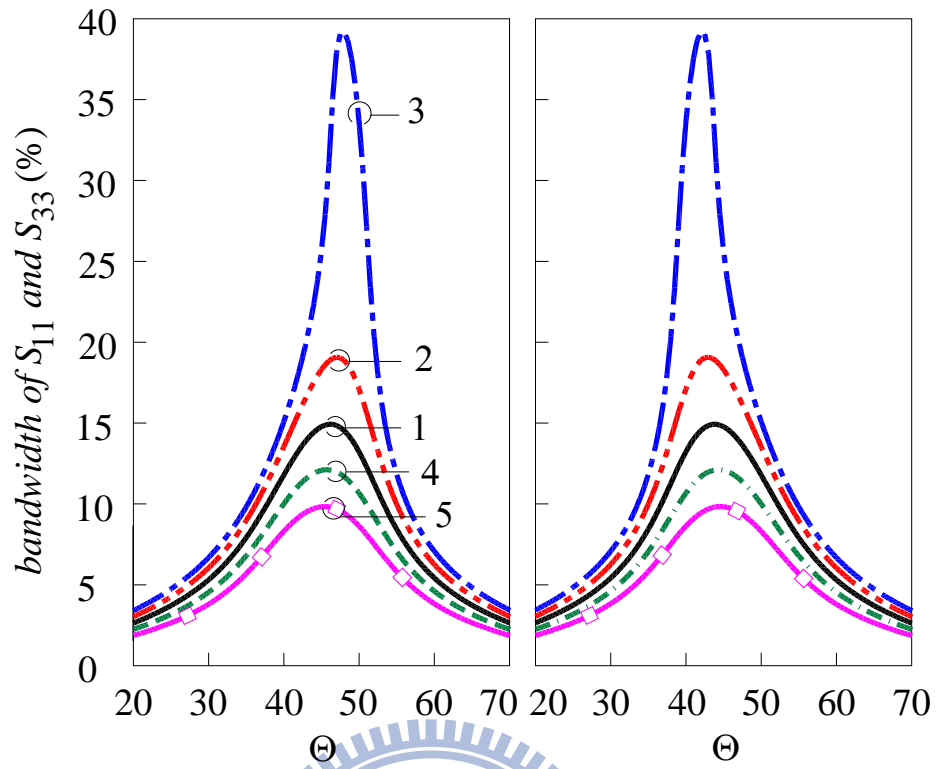


(d)

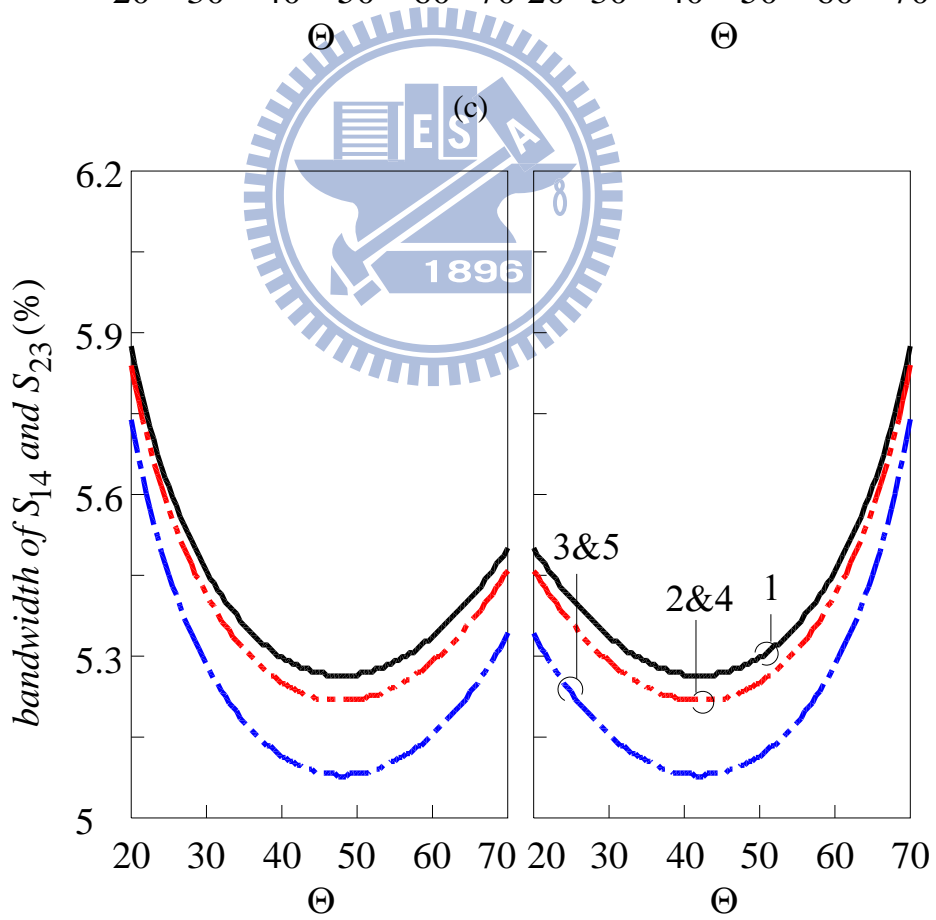
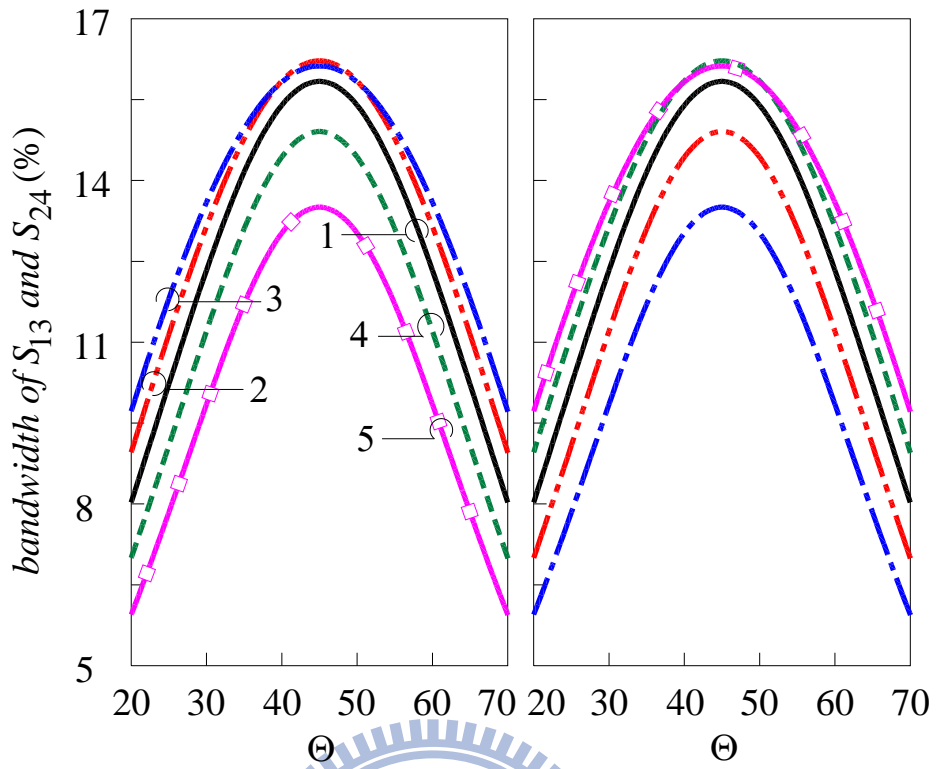


(e)

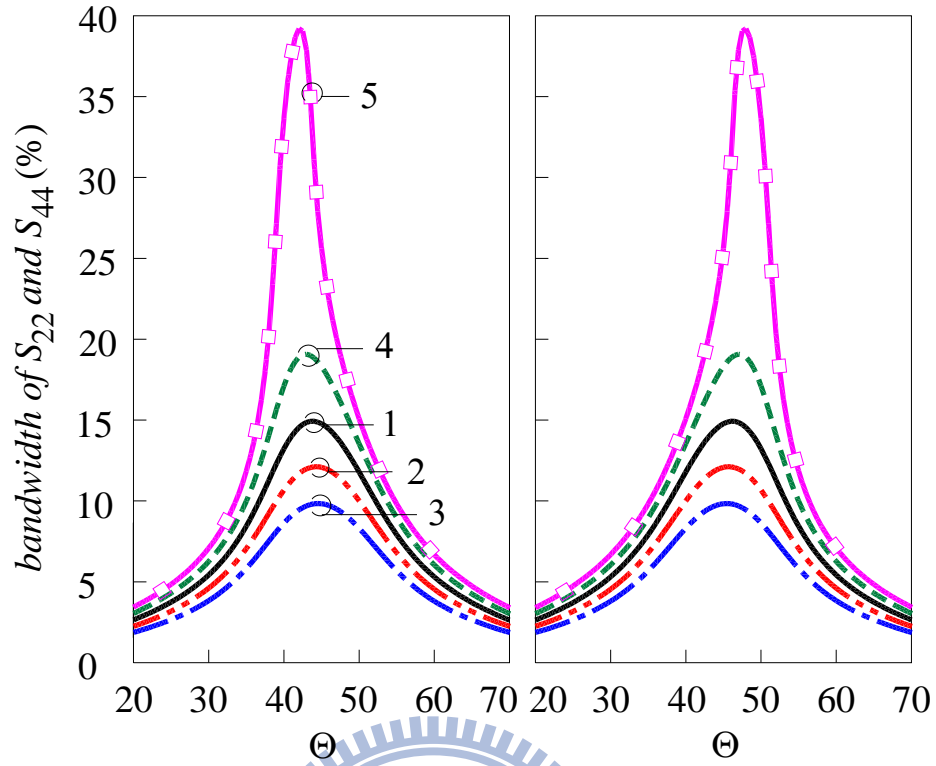
Figure 2.7 Bandwidths measured by S -parameter responses. Port 1 and port 3 are terminated in Z_{01} and port 2 and port 4 are terminated in Z_{02} . $Z_{i1} = Z_{i2} = Z_{02}$. Curves 1 ~ 5 have $Z_{01}:Z_{02} = 1:1, 1:2, 1:4, 2:1, \text{ and } 4:1$, respectively. (a) $|S_{11}|$ and $|S_{33}|$. (b) $|S_{21}|$ and $|S_{34}|$. (c) $|S_{13}|$ and $|S_{24}|$. (d) $|S_{14}|$ and $|S_{23}|$. (e) $|S_{22}|$ and $|S_{44}|$.



(b)



(d)



(d)

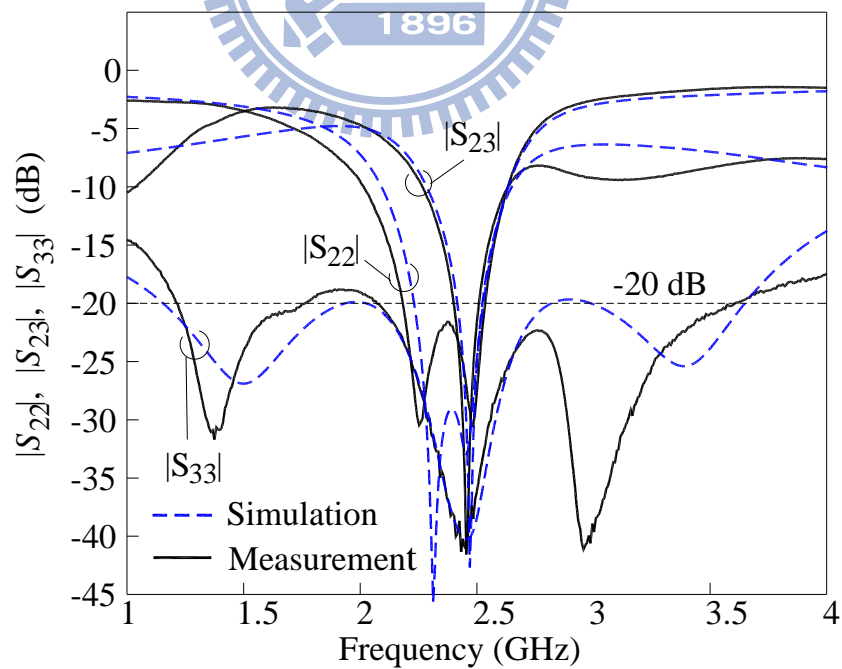
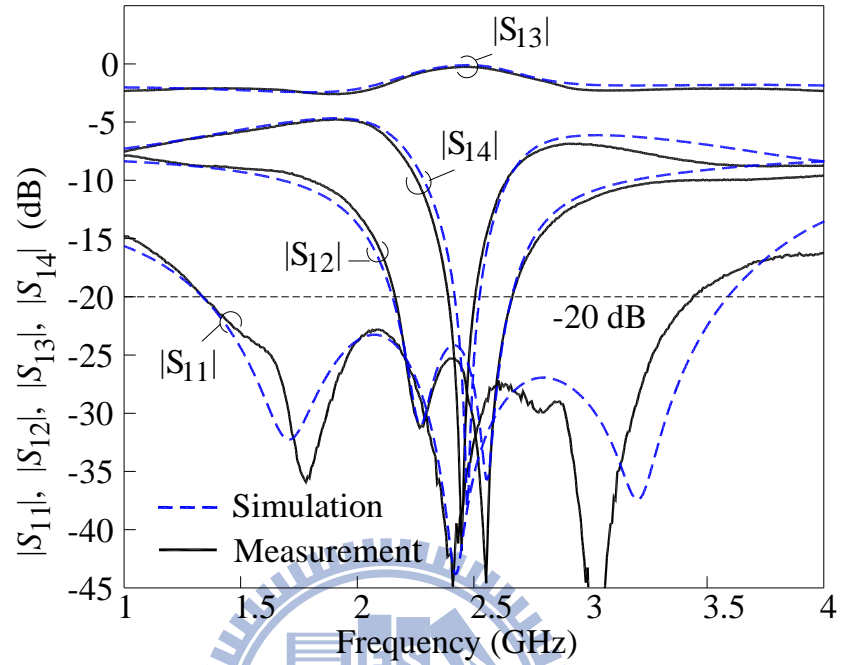
Figure 2.8 Bandwidths measured by S -parameter responses. Port 1 and port 3 are terminated in Z_{01} and port 2 and port 4 are terminated in Z_{02} . $Z_{i1} = Z_{i2} = \sqrt{Z_{01}Z_{02}}$. Curves 1 ~ 5 have $Z_{01}:Z_{02} = 1:1, 1:2, 1:4, 2:1, \text{ and } 4:1$, respectively. (a) $|S_{11}|$ and $|S_{33}|$. (b) $|S_{21}|$ and $|S_{34}|$. (c) $|S_{13}|$ and $|S_{24}|$. (d) $|S_{14}|$ and $|S_{23}|$. (e) $|S_{22}|$ and $|S_{44}|$.

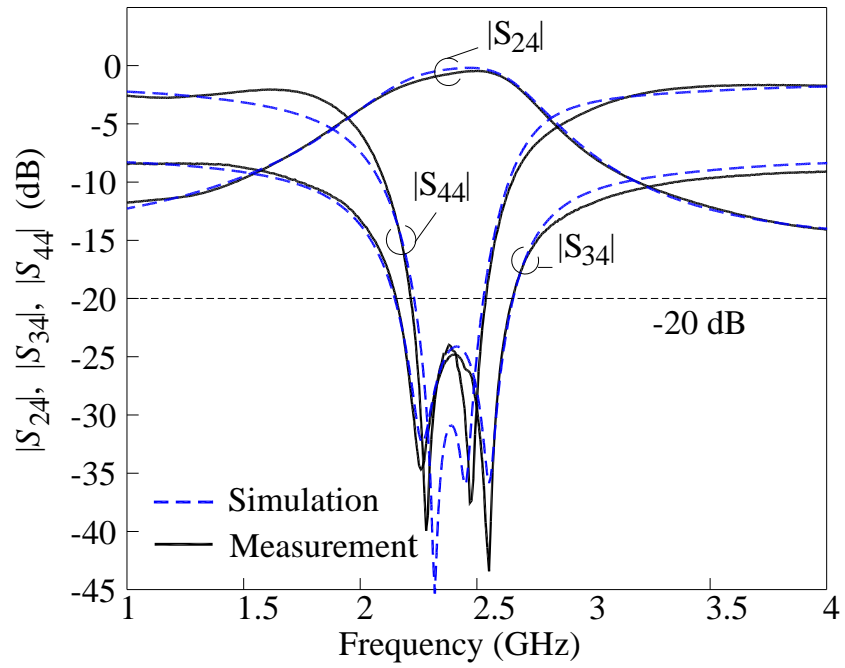
2.3 Simulation and Measurement

Two circuits are fabricated and measured to validate the design. Figure 2.9 (a) ~ (c) plot the simulation and measurement of the first fabricated circuit with $Z_{o1} = 25 \Omega$, $Z_{o2} = 100 \Omega$, $Z_i = 100 \Omega$ and $\Theta = 46^\circ$. The center frequency is designed at 2.45 GHz. The circuit simulation is done by the software package IE3D [20]. The substrate has $\epsilon_r = 10.2$ and $h = 1.27$ mm. The S -parameters are measured with reference port impedance 50Ω . The measured data are converted to S -parameters with designated port impedances with the aids of Y -parameters. If a 20-dB return loss, 0.5dB insertion loss and 20-dB isolation are referred, the estimation bandwidths are shown as curve 3 of Figure 2.7. The estimated bandwidths of $|S_{11}|$, $|S_{21}|$, $|S_{31}|$, $|S_{41}|$, $|S_{22}|$, $|S_{23}|$, $|S_{24}|$, $|S_{33}|$, $|S_{34}|$ and $|S_{44}|$ are 92.9%, 16.5%, 13.4%, 4.1%, 10.3%, 4.1%, 12.2%, 23.4%, 16.3% and 10.4%. Figure 2.9 (a)~(c) show the simulation IE3D bandwidths of $|S_{11}|$, $|S_{21}|$, $|S_{31}|$, $|S_{41}|$, $|S_{22}|$, $|S_{23}|$, $|S_{24}|$, $|S_{33}|$, $|S_{34}|$ and $|S_{44}|$ are 92%, 21%, 13.3%, 4.3%, 12.1%, 4.4%, 10.2%, 32.5%, 20.7% and 12.1% and the measured responses have 85.7%, 20.5%, 10.4%, 4.9%, 14.4%, 4.3%, 3.7%, 62.4%, 20.5% and 13.1% respectively. The measured data has good agreement with the simulation and the calculation. Figure 2.9 (d) shows the photo of the experimental circuit.

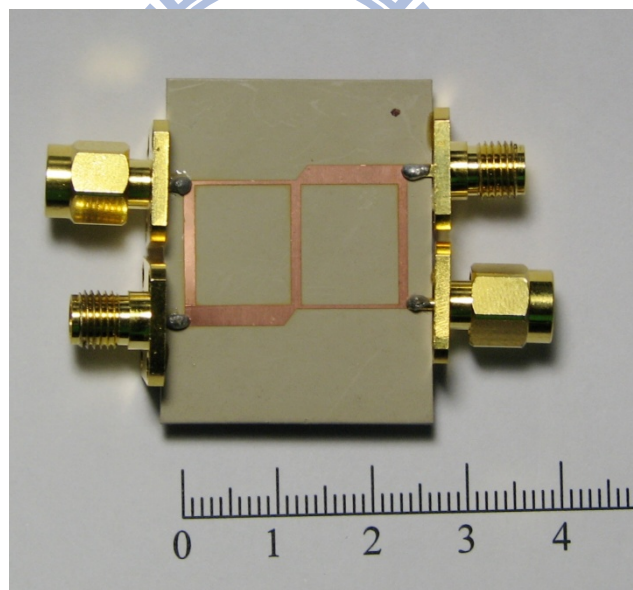
Figure 2.10 (a) ~ (c) plot the simulation and measurement results of the second fabricated circuit with $Z_{o1} = 100 \Omega$, $Z_{o2} = 50 \Omega$, $Z_i = 50 \Omega$ and $\Theta = 40^\circ$. Again, a 20-dB return loss, 0.5dB insertion loss and 20-dB isolation are referred, and the estimation bandwidths are shown as curve 4 in Figure 2.6. The calculated bandwidths of $|S_{11}|$, $|S_{21}|$, $|S_{31}|$, $|S_{41}|$, $|S_{22}|$, $|S_{23}|$, $|S_{24}|$, $|S_{33}|$, $|S_{34}|$ and $|S_{44}|$ are 9.48%, 17.5%, 14.8%, 5.8%, 15.36%, 5.74%, 16.73%, 9.98%, 16.87% and 12.9%, respectively. Figure 2.10 (a)~(c) show the simulation bandwidths of $|S_{11}|$, $|S_{21}|$, $|S_{31}|$, $|S_{41}|$, $|S_{22}|$, $|S_{23}|$, $|S_{24}|$, $|S_{33}|$, $|S_{34}|$ and $|S_{44}|$ are 10.36%, 19.12%, 12.86%, 5.79%, 18.06%, 5.73%, 15.25%, 11.09%, 18.72% and 14.53% and the measured results have 11.63%, 19.59%, 6.43%, 5.51%, 15.31%, 6.12%, 11.94%, 14.39%, 18.98% and 14.08%, respectively.

The measured responses have good agreement with the simulation and calculation. Figure 2.10 (d) shows the photo of the realized circuit.



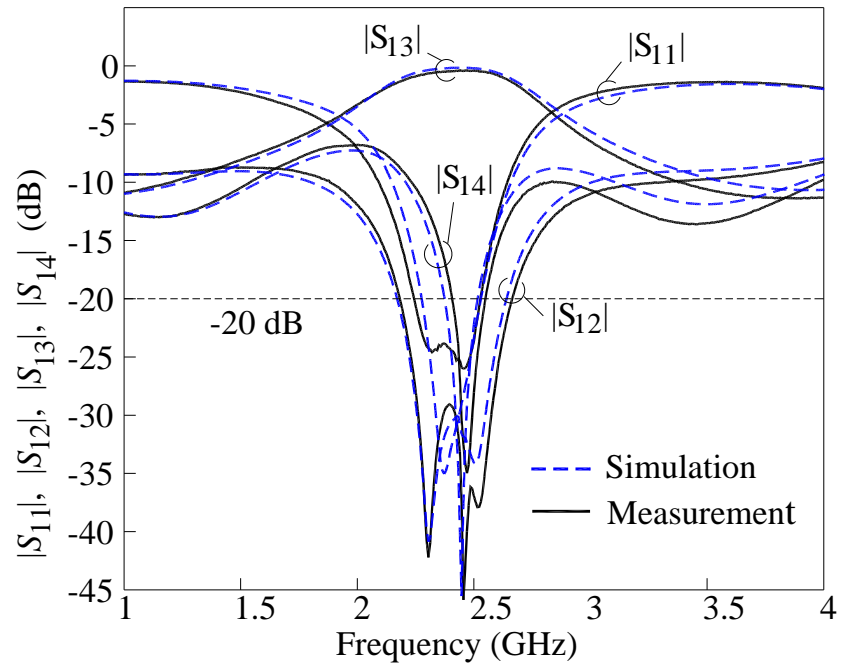


(c)

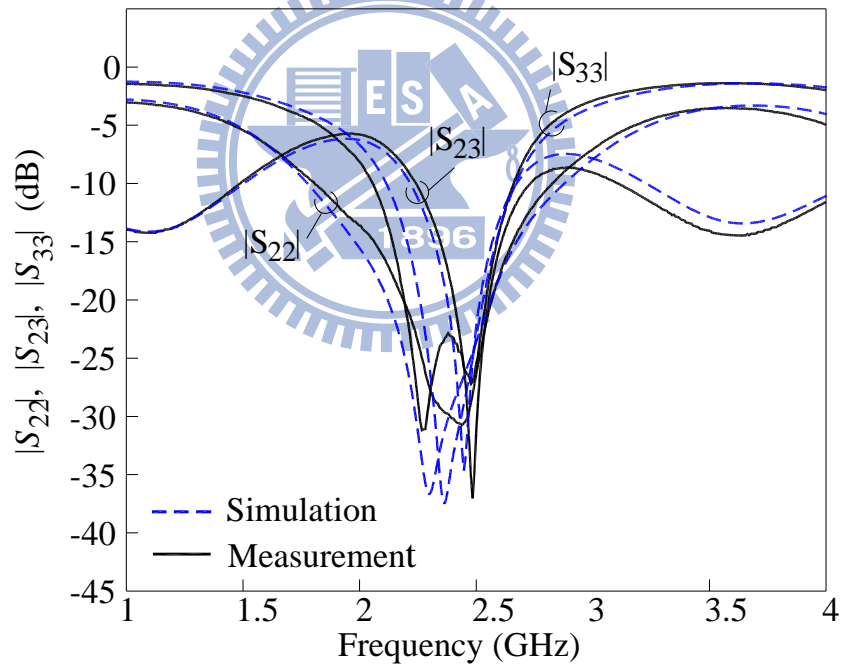


(d)

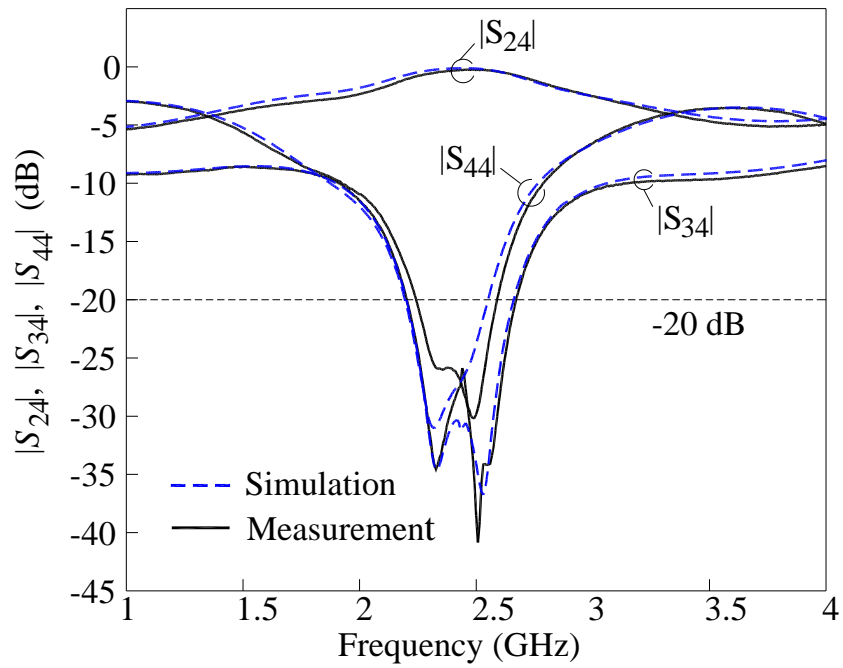
Figure 2.9 The S -parameters of the first fabricated circuit with $Z_{o1} = 25 \Omega$, $Z_{o2} = 100 \Omega$, $Z_i = 100 \Omega$ and $\Theta = 46^\circ$. (a) $|S_{11}|$, $|S_{21}|$, $|S_{31}|$, $|S_{41}|$. (b) $|S_{22}|$, $|S_{23}|$, $|S_{33}|$. (c) $|S_{24}|$, $|S_{34}|$, $|S_{44}|$. (d) The circuit photo. $W_1 \sim W_7$ are 2.06, 0.48, 1.01, 1.1, 1.18, 0.43 and 2.19 mm. $L_1 \sim L_7$ are 11.06, 11.69, 11.42, 11.39, 11.35, 11.72 and 11.02 mm.



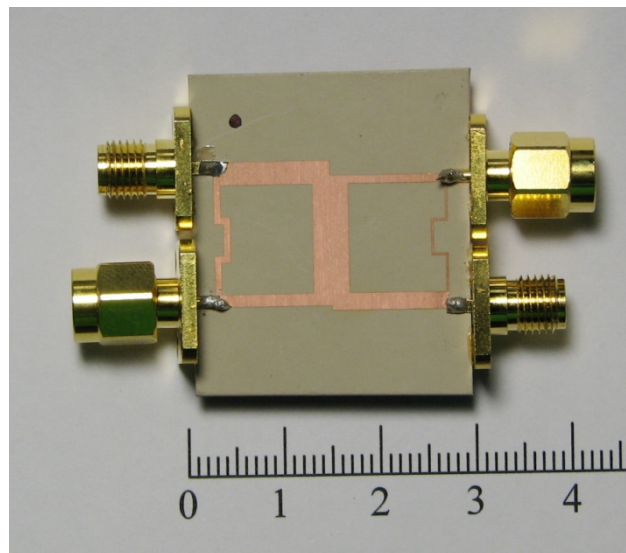
(a)



(b)



(c)



(d)

Figure 2.10 The S -parameters of the second fabricated circuit with $Z_{o1} = 100 \Omega$, $Z_{o2} = 50 \Omega$, $Z_i = 50 \Omega$ and $\Theta = 40^\circ$. (a) $|S_{11}|$, $|S_{21}|$, $|S_{31}|$, $|S_{41}|$. (b) $|S_{22}|$, $|S_{23}|$, $|S_{33}|$. (c) $|S_{24}|$, $|S_{34}|$, $|S_{44}|$. (d) Circuit photo. $W_1 \sim W_7$ are 1.33, 1.84, 0.74, 3.74, 0.26, 2.49 and 0.92 mm. $L_1 \sim L_7$ are 11.29, 11.12, 11.55, 10.7, 11.85, 10.95 and 11.47 mm.

Chapter 3

Dual-Band Crossover Coupler Design

Recent rapid progress in wireless communications has created a need of dual-band operation for RF devices, such as the global systems for mobile communication systems (GSM) at 0.9/1.8 GHz and wireless local area network (WLAN) at 2.4/5.2 GHz. This Chapter studies the design of crossover coupler with dual-band operation.

3.1 Elementary Two-Port for Dual-Band Operation

Figure 3.1 shows the elementary two-port for substituting a $\lambda/4$ -section to achieve dual-band operation. The elementary two-port consists of two high-Z sections on both sides with two stubs being attached to their ends and a low-Z section in the middle. Let the admittance of the two shunt stubs be $jB/2$. Since the circuit is symmetric about its center, by setting the reference plane in the middle open- and short-circuited, respectively, the input admittances for even- and odd-mode, $y_e = y_{11} + y_{21}$ and $y_o = y_{11} - y_{21}$, can be readily derived as follows:

$$y_{11} + y_{21} = j\frac{B}{2} + j\frac{1}{Z_1} \frac{R \tan \theta_{s2} + \tan \theta_{s1}}{1 - R \tan \theta_{s1} \tan \theta_{s2}} \quad (3.1a)$$

$$y_{11} - y_{21} = j\frac{B}{2} + j\frac{1}{Z_1} \frac{-R \cot \theta_{s2} + \tan \theta_{s1}}{1 + R \tan \theta_{s1} \cot \theta_{s2}} \quad (3.1b)$$

Let the two designated operation frequencies be f_1 and $f_2 = \eta f_1$. To have the crossover junction operate with a dual-passband characteristic, each $\lambda/4$ -section of the two asymmetric branch-line hybrids is replaced by the elementary two-port network, which is capable of providing 90 and 270 degrees at f_1 and f_2 , respectively. The following equations can be derived.

$$y_{21}(f_1) = (P(\theta_{s1}, \theta_{s2}) - Q(\theta_{s1}, \theta_{s2})) / 2 = Z_{s1} / Z_T \quad (3.2a)$$

$$y_{21}(nf_1) = (P(\theta_{s1}, \theta_{s2}) - Q(\theta_{s1}, \theta_{s2})) / 2 = Z_{s1} / Z_T \quad (3.2b)$$

$$Z_{s1} \times B(f_1) = -(P(\theta_{s1}, \theta_{s2}) + Q(\theta_{s1}, \theta_{s2})) \quad (3.2c)$$

$$Z_{s1} \times B(nf_1) = -(P(\theta_{s1}, \theta_{s2}) + Q(\theta_{s1}, \theta_{s2})) \quad (3.2d)$$

where

$$P(\phi, \varphi) = \frac{\tan \phi + R \tan \varphi}{1 - R \tan \phi \tan \varphi} \quad (3.3a)$$

$$Q(\phi, \varphi) = \frac{\tan \phi - R \cot \varphi}{1 + R \tan \phi \cot \varphi} \quad (3.3b)$$

where $R = Z_{s1}/Z_{s2}$, Z_T can be the characteristic impedance of the $\lambda/4$ -section, and $B/2$ is the susceptance of the shunt open stub. $y_{21}(f_1) = \text{Im}[Y_{21}(f_1) \times Z_1]$ and $y_{21}(nf_1) = \text{Im}[Y_{21}(nf_1) \times Z_1]$ represent respectively the normalized (2, 1) entry of the Y -matrix of the two-port at f_1 and $f_2 = nf_1$. Fig. 3.2(a) and (b) plot both $y_{21}(f_1)$ and $y_{21}(nf_1)$ curves against θ_{s1} for various R values when $\theta_{s2} = 5^\circ$ and 10° , respectively. Both θ_{s1} and θ_{s2} are evaluated at f_1 . For each R , the intersection point of the $y_{21}(f_1)$ and $y_{21}(nf_1)$ curves gives the solution. Inserting these solutions into (3.2c) and (3.2d), values of $B(f_1)$ and $B(nf_1)$, and hence the electrical length and characteristic impedance of open stubs, can be obtained.

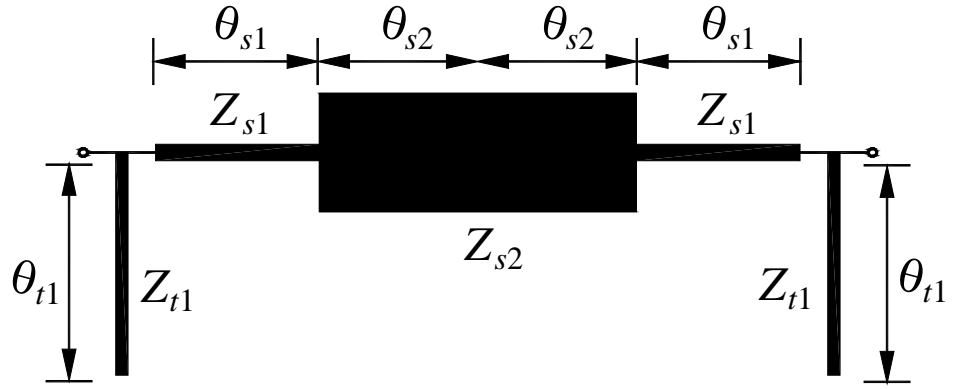
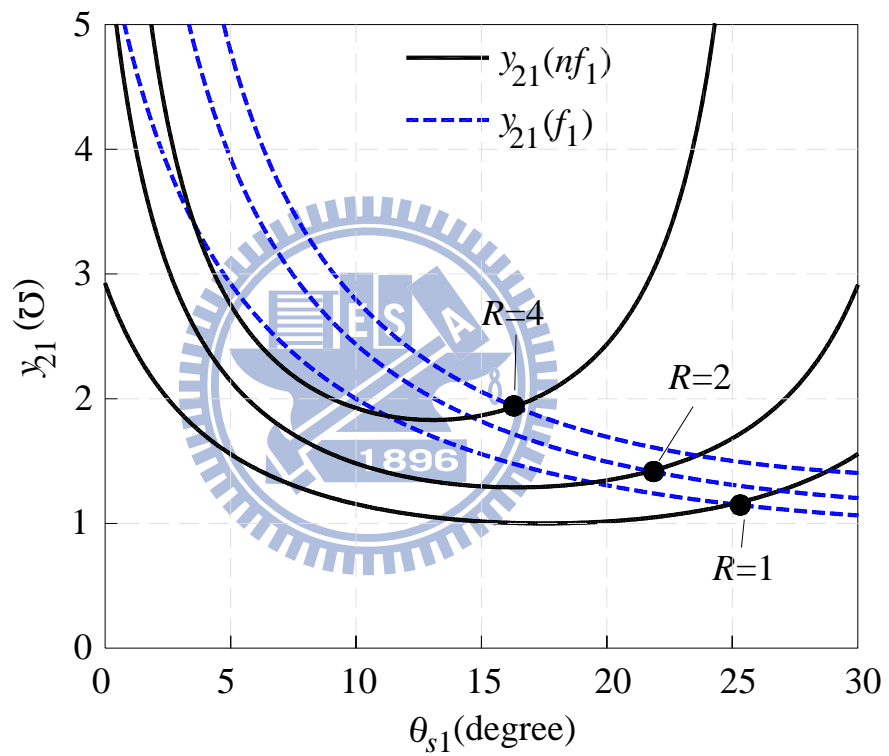


Figure 3.1 Two-port network for substituting a quarter-wave section.



(a)

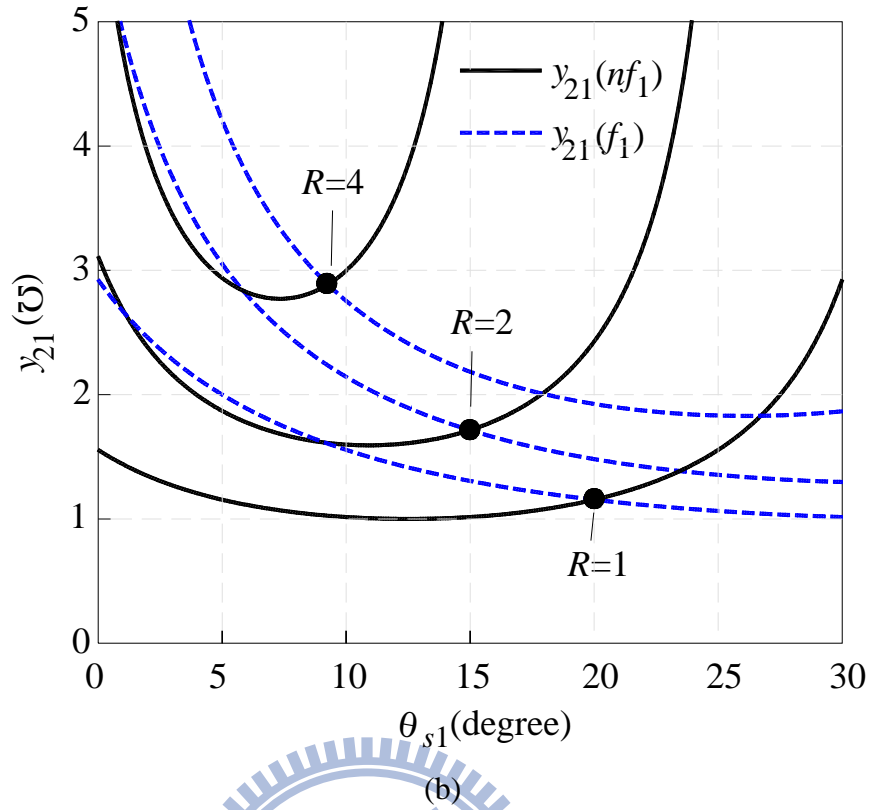


Figure 3.2 Design graphs for determining θ_{s1} and R . (a) $\theta_{s2} = 5^\circ$. (b) $\theta_{s2} = 10^\circ$. Both θ_{s1} and θ_{s2} values are referred to f_1 .

3.2 Simulation and Measurement

A microstrip crossover coupler designed at 0.9/1.8 GHz is fabricated and measured for demonstration. The circuit is built on a substrate of $\epsilon_r = 10.2$ and $h = 0.508$ mm. The characteristic impedances of the branches in Figure 3.3 are $Z_{a1} = 39.36 \Omega$, $Z_{b1} = 33.17 \Omega$, $Z_{a2} = 29.67 \Omega$, $Z_{a3}/Z_{b2} = 36.93 \Omega$, $Z_{b3} = 42.13 \Omega$, $Z_{a4} = 27.83 \Omega$, and $Z_{b4} = 46.91 \Omega$. Termination impedances of the port 1 and port 3 are Z_{o1} and these of the port 2 and port 4 are Z_{o2} . Each branch is substituted by the two-port in Fig. 3.1 by using the solutions in Fig. 3.2(b) with $R = 2$, $\theta_{s1} = 15^\circ$ and $\theta_{s2} = 10^\circ$.

Figure 3.4 compares the measured results with the simulation data obtained by the IE3D [18]. Figure 3.4(a) and 3.4(b) plots the circuit responses when port 1 is excited, and 3.4(c) and 3.4(d) draws the results when signal is fed to port 2. In Fig. 3.4(a), it can

be observed that the measured return losses $|S_{11}|$ and the isolations $|S_{41}|$ at the two designated frequencies are better than -20 dB. If a 15-dB return loss is referred, measured data indicate that $|S_{11}|$ has bandwidths of 10.8% and 4.6% and $|S_{11}|$ has 3.5% and 4.2% at f_1 and f_2 , respectively. Fig. 3.4(b) shows the isolation between port 2 and port 1 $|S_{21}|$ and the crossover response $|S_{31}|$. The measured $|S_{31}| = -0.89$ dB and -1.1 dB at f_1 and f_2 , respectively. When input is at port 2, the measured return loss $|S_{22}|$ in Fig. 3.4(c) is better than -20 dB and has bandwidths of 15% and 5.8% at f_1 and f_2 , respectively, for a 15-dB reference. The experimental $|S_{32}|$ indicate that the isolations between ports 2 and 3 are better than 20 dB in both bands. In Fig. 3.4(d), the measured $|S_{42}| = -0.69$ dB and -1.24 dB at f_1 and f_2 , respectively. In Fig. 3.4(a) through 3.4(d), reasonably good agreement between the simulation and measurement can be observed. Fig. 3.4(e) shows the photograph of the experimental four-port dual-band crossover junction.

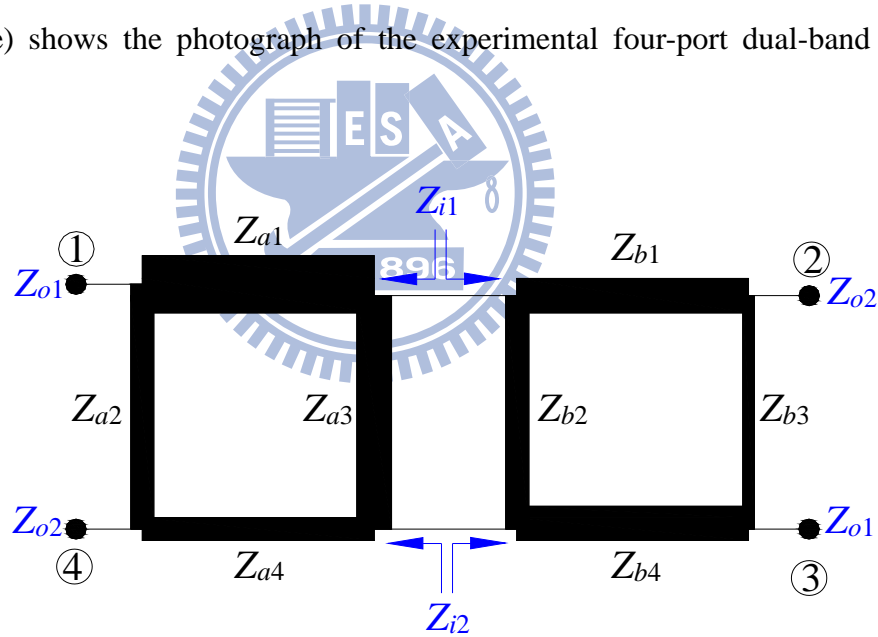
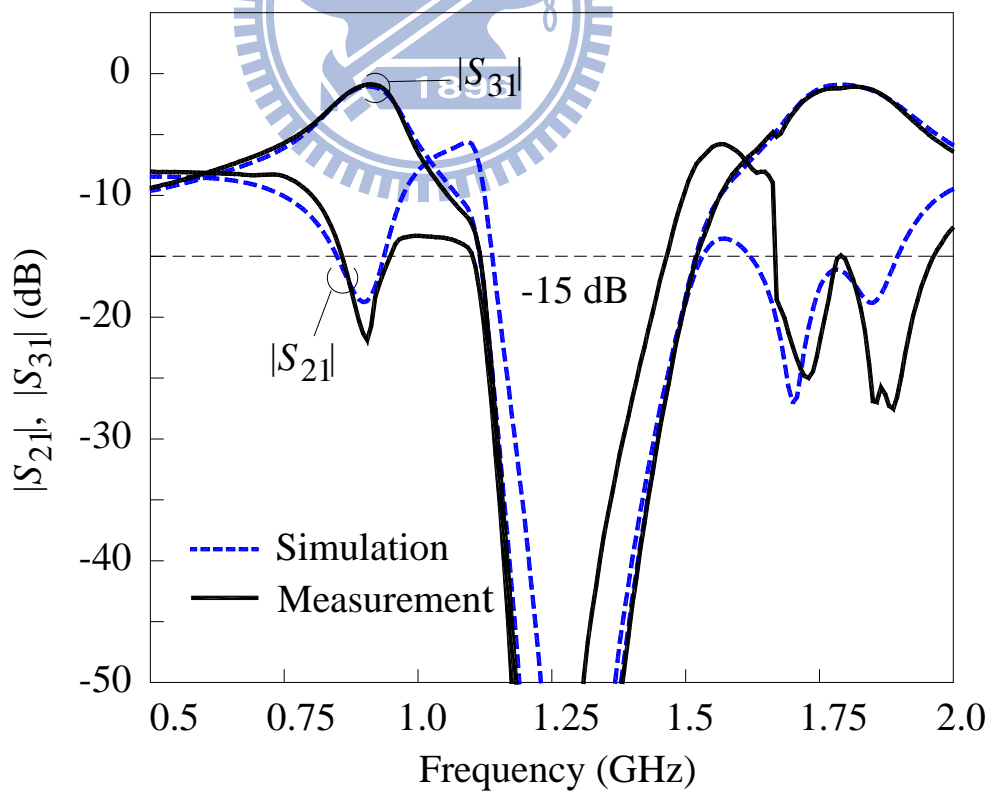
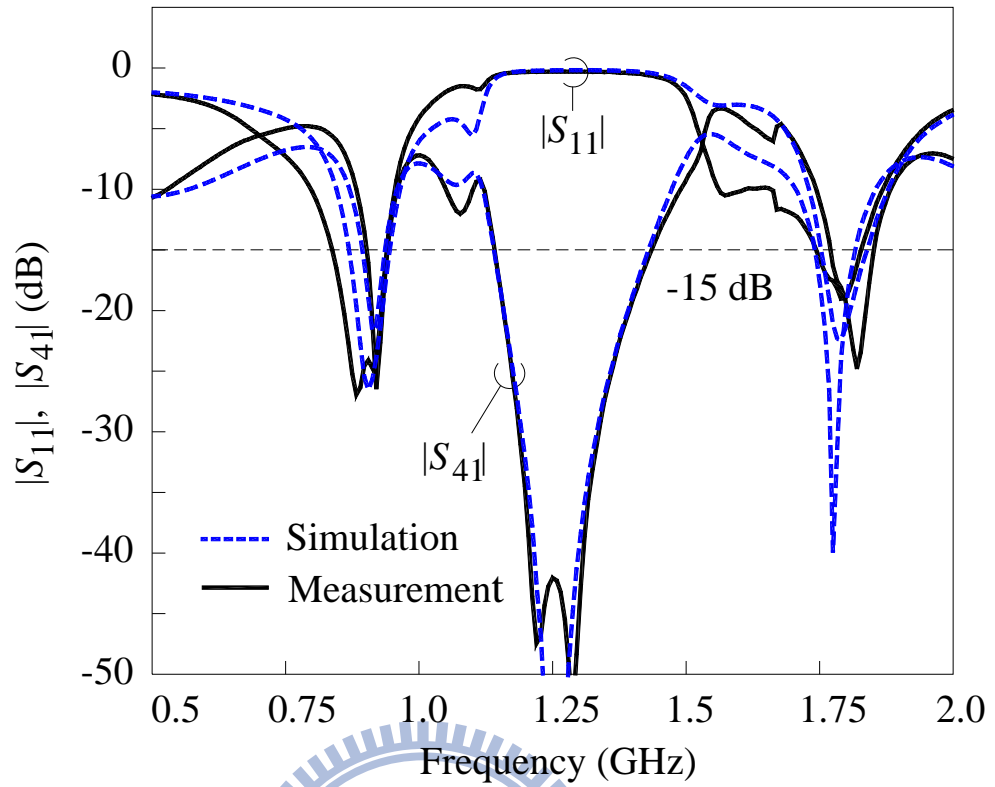
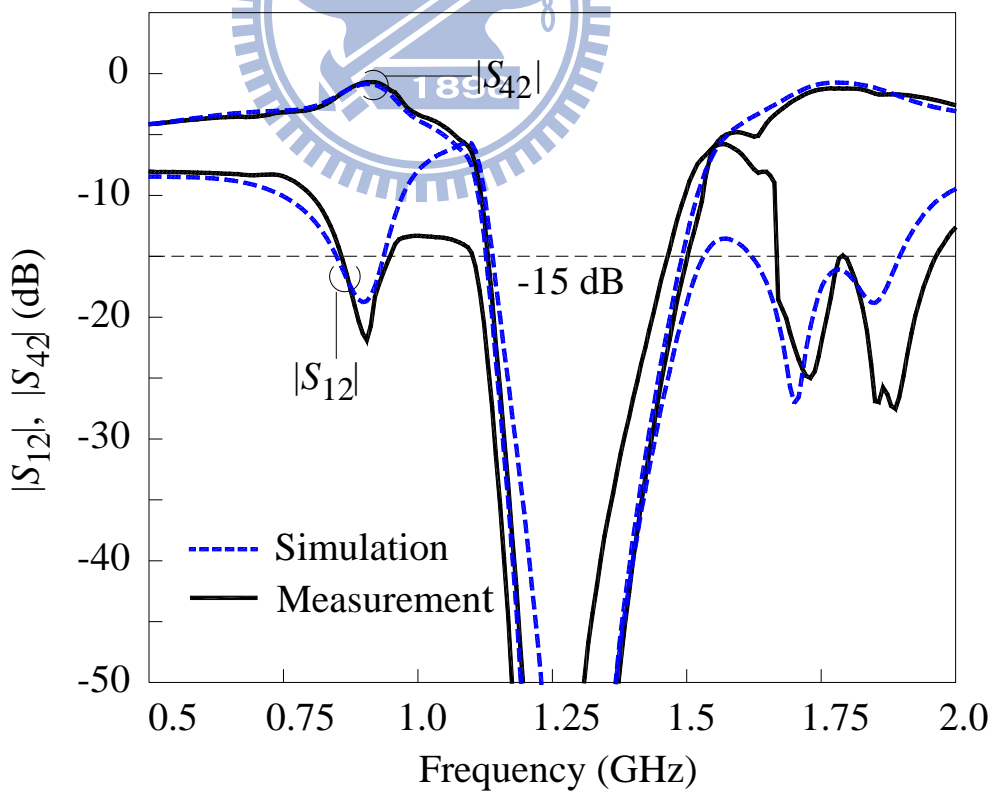
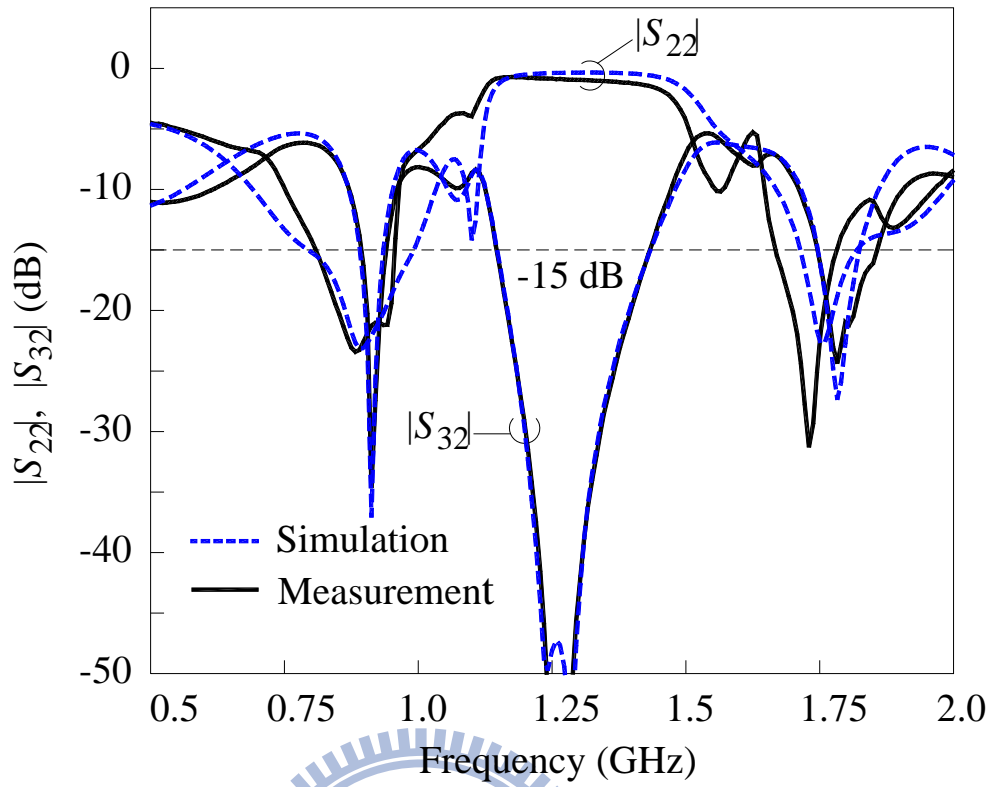


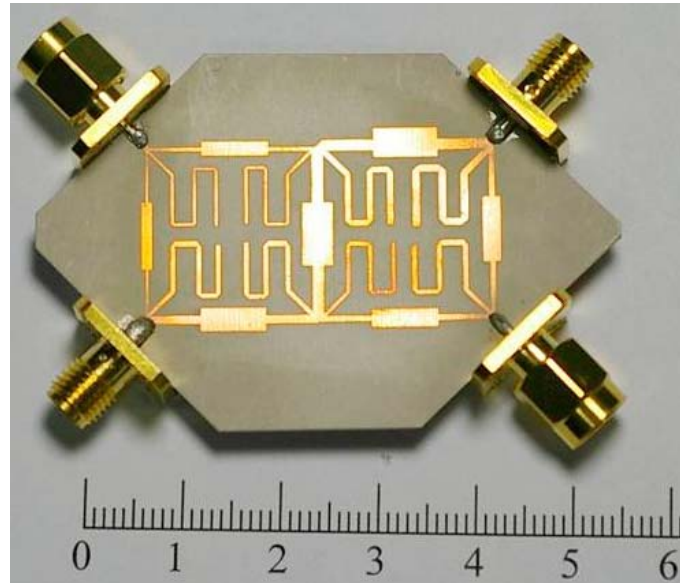
Figure 3.3 Two cascaded asymmetric branch-line hybrids to form a new crossover coupler with arbitrary diagonal port impedances Z_{o1} and Z_{o2} .



(b)



(d)



(e)

Figure 3.4 Simulation and measured responses of the fabricated dual-band crossover junction. (a) $|S_{11}|$ and $|S_{41}|$. (b) $|S_{21}|$ and $|S_{31}|$. (c) $|S_{22}|$ and $|S_{32}|$. (d) $|S_{12}|$ and $|S_{42}|$. $Z_{o1} = 50 \Omega$ and $Z_{o2} = 25 \Omega$. (e) Photograph of the experimental circuit.



Chapter 4

Conclusion

A new design for crossover coupler with different diagonal port impedances is devised by using a cascade of asymmetric branch-line couplers with arbitrary power division. It allows the port termination impedances to be arbitrary. Circuit analysis in term of block $ABCD$ matrix and Y -matrix formulation is used to calculate the bandwidth associated with each S -parameter. In the second part of this thesis, the crossover is devised to have dual-band operation. Each quarter-wave section is replaced by an elementary two-port shown which is designed to achieve proper phase changes at the two designated frequencies. One microstrip circuit for operation at 0.9/1.8 GHz is realized. The measured responses not only validate the idea but also agree well with the simulation.

There is still some room for improving the performance of the proposed crossover couplers. First, is it possible to synthesize a passband of crossover couplers like a filter? The passband function can be maximally flat response, Butterworth response or elliptic function response. Furthermore, the size of a microstrip realization can be too large to be used in some applications. It needs miniaturizing circuit size and keeping the flexibility of the port termination impedances at the same time. Second, if a passband response can be synthesized for a crossover coupler, many existing design techniques for dual-band bandpass filter can be useful for microwave passive circuit.

References

- [1] T.-S. Hong, "A rigorous study of microstrip crossovers and their possible improvements," *IEEE Trans. Microw. Theory Tech.*, vol. 42, no. 9, pp. 1802-1806, Sep. 1994.
- [2] C.-C. Chang, T.-Y. Chin, J.-C. Wu and S.-F. Chang, "Novel design of a 2.5-GHz fully integrated CMOS Butler matrix for smart-antenna systems," *IEEE Trans. Microw. Theory Tech.*, vol. 56, no. 8, pp. 1757 - 1763, Aug. 2008.
- [3] J. S. Wight, W. J. Chudobiak and V. Makios, "A microstrip and stripline crossover structure," *IEEE Trans. Microw. Theory Tech.*, vol. 24, no. 5, pp. 270, May 1976.
- [4] F. C. de Ronde, "Octave-wide matched symmetrical, reciprocal, 4- and 5 ports," in *IEEE MTT-S Int. Microw. Symp. Dig.*, pp. 521–523, Jun.1982.
- [5] K. C. Gupta and M. D. Abouzahra, "Analysis and design of four-port and five-port microstrip disk circuits," *IEEE Trans. Microw. Theory Tech.*, vol. 33, no. 12, pp. 1422-1428, Dec. 1985.
- [6] D. V. Kholodniok and I. Vendik, "A novel type of 0-dB directional coupler for microwave integrated circuits," in *29th European Microw. Conf.*, pp. 341-344, Nov. 1999.
- [7] D. V. Kholodniok, G. Kalinin, E. Vernoslova, and I. Vendik, "Wideband 0-dB branch-line directional couplers," in *IEEE MTT-S Int. Microw. Symp. Dig.*, pp. 1307–1310, Jun. 2000.
- [8] Y. Chen and S.-P. Yeo, "A symmetrical four-port microstrip coupler for crossover application," *IEEE Trans. Microw. Theory Tech.*, vol. 55, no. 11, pp. 2434-2438, Nov. 2007.
- [9] Y.-C. Chiou, C.-H. Tsai and J.-T. Kuo, "Comments on "A symmetrical four-port microstrip coupler for crossover application," " *IEEE Trans. Microw. Theory Tech.*, vol. 57, no. 7, pp. 1859-1860, July. 2009.

- [10] Y.-C. Chiou, J.-T. Kuo and H.-R. Lee, "Design of compact symmetric four-port crossover junction," *IEEE Microw. Wireless Component Letters*, vol. 19, no. 9, pp. 545-547, September 2009.
- [11] H.-R. Ahn, I. Wolff and I.-S. Chang, "Arbitrary termination impedances, arbitrary power division, and small-sized ring hybrids," *IEEE Trans. Microw. Theory Tech.*, vol. 45, no. 12, pp. 2241-2247, Dec. 1997.
- [12] H.-R. Ahn and I. Wolff, "Asymmetric four-port and branch-line hybrids," *IEEE Trans. Microw. Theory Tech.*, vol. 48, no. 9, pp. 1585-1588, Sep. 2000.
- [13] J.-T. Kuo, T.-H. Yeh and C.-C. Yeh, "Design of microstrip bandpass filters with a dual-passband response," *IEEE Trans. Microwave Theory Tech.*, vol. MTT-53, no. 4, pp. 1331-1337, Apr. 2005.
- [14] K.-K. M. Cheng and F.-L. Wong, "A novel approach to the design and implementation of dual-band compact planar 90° branch-line coupler," *IEEE Trans. Microw. Theory Tech.*, vol. 52, no. 11, pp. 2458-2463, Nov. 2004.
- [15] C.-L. Hsu, J.-T. Kuo and C.-W. Chang, "Miniaturized dual-band hybrid couplers with two arbitrary power division ratios," *IEEE Trans. Microwave Theory Tech.*, vol. MTT-57, no. 1, pp. 149-156, Jan. 2009.
- [16] I.-H. Lin, M. Devincenstis, C. Caloz and T. Itoh, "Arbitrary dual-band components using composite right/left-handed transmission lines," *IEEE Trans. Microw. Theory Tech.*, vol. 52, no.4, pp. 1142-1149, Apr. 2004.
- [17] C. Monzon, "A small dual-frequency transformer in two sections," *IEEE Trans. Microw. Theory Tech.*, vol. 51, no. 4, pp. 1157-1161, Apr. 2003.
- [18] S. Srisathit, M. Chongcheawchamnan, and A. Worapishet, "Design and realization of dual-band 3 dB power divider based on two-section transmission-line topology," *IEE Electronics Lett.*, vol. 39, no. 9, pp. 723-724, May 2003.
- [19] Yu-Shin Wang, Ming-Chou Lee, and Shyh-Jong Chung, "Two PIFA-Related Miniaturized Dual-Band Antennas," *IEEE Trans. Antennas Propagat.*, Vol. 55, No. 3, Mar. 2007

[20] *Matlab R2008a*. The MathWorks Inc., Feb. 2008.

